A&A 492, 493–509 (2008)
DOI: 10.1051/0004-6361:20078798


Astronomy & Astrophysics

# A consistent solution for the velocity field and mass-loss rate of massive stars

P. E. Müller[1] and J. S. Vink[2]

[1] School of Physical and Geographical Sciences, Lennard-Jones Laboratories, Keele University, Staffordshire ST5 5BG, UK
e-mail: pmueller@astro.keele.ac.uk
[2] Armagh Observatory, College Hill, Armagh BT61 9DG, Northern Ireland, UK

Received 5 October 2007 / Accepted 7 October 2008

**ABSTRACT**

Stellar winds are an important aspect of our understanding of the evolution of massive stars and their input into the interstellar medium. Here we present solutions for the velocity field and mass-loss rates for stellar outflows as well as for the case of mass accretion through the use of the so-called Lambert *W*-function. For the case of a radiation-driven wind, the velocity field is obtained analytically using a parameterised description for the line acceleration that only depends on radius, which we obtain from Monte-Carlo multi-line radiative transfer calculations. In our form of the equation of motion the critical point is the sonic point. We also derive an approximate analytical solution for the supersonic flow which closely resembles our exact solution. For the simultaneous solution of the mass-loss rate and velocity field, we describe a new iterative method. We apply our theoretical expressions and our iterative method to the stellar wind from a typical O5-V main sequence star, and find good agreement with empirical values. Our computations represent a self-consistent mass-loss calculation including the effect of multi-line scattering for an O-type star, opening up the possibility of applying Monte Carlo mass-loss calculations in regions of the Universe for which empirical constraints cannot be readily obtained.

**Key words.** hydrodynamics – methods: analytical – methods: numerical – stars: early-type – stars: mass-loss – stars: winds, outflows

## 1. Introduction

Stellar winds are crucial for our understanding of the evolution of massive stars towards their final explosion. Furthermore, mass loss constitutes an important source of chemical enrichment into the interstellar medium. As we cannot obtain observations of individual stars at high redshift, we need to develop a theoretical framework that works locally and which confidently can be applied to the early Universe. Developing such a framework is the aim of this paper.

That the winds from massive O stars are driven by radiation pressure through spectral lines has been known since the seminal papers of Lucy & Solomon (1970) and Castor et al. (1975, hereafter CAK). Currently, there are two basic methods in use to compute the mass-loss rates of massive stars. These involve a modified version of the CAK method (Pauldrach et al. 1986; Kudritzki 2002) and the Monte Carlo method (Abbott & Lucy 1985; Vink et al. 2000). The *pros* and *cons* of these two distinct approaches have recently been reviewed by Vink (2006).

A common feature of supersonic flows are critical points. Within the CAK framework, the wind velocity, $v(r)$, has critical points defined by three singularity conditions, whilst assuming a power-law for the line acceleration, to obtain an approximate solution of the equation of motion. To solve this equation, CAK attributed the same status to the Sobolev velocity derivative as to the Newtonian derivative. This CAK *ansatz* was immediately criticised by Lucy (1975, 1998, 2007b; see also Vink et al. 1999; Vink 2000), but the CAK-scaling relations have been widely used, presumably because of their reasonable agreement with observations. The analyses of continuum emission and line profiles yielded mass-loss rates $\dot{M}$ from $10^{-6}$ to $10^{-5}$ $M_\odot$/year, and terminal velocities of about three times the escape velocity, $\sim$3000 km s$^{-1}$ for a main-sequence O-star (e.g. Howarth & Prinja 1989). That the CAK predictions are in rough agreement with observations at all is largely fortuitous (see Vink 2006), as the assumptions of local thermodynamic equilibrium and the early use of limited line lists are a posteriori known to be insufficient. The CAK framework itself however has proved to be very successful and improvements in non-LTE radiative transfer as well as atomic data have led to more reliable predictions by e.g. Pauldrach et al. (1986). Nevertheless, even these modified CAK scaling relations have not been able to reproduce the mass-loss rates of the denser O star winds (Lamers & Leitherer 1993; Vink et al. 2000), nor the winds of Wolf-Rayet stars (Lucy & Abbott 1993; Gayley 1995; Gräfener et al. 2002; Gräfener & Hamann 2005).

For this reason, an alternative method for predicting mass-loss rates, the Monte Carlo (MC) technique, was developed (Abbott & Lucy 1985; Puls 1987; Schmutz 1997; de Koter et al. 1997; Vink et al. 1999). The MC approach does not rely on the CAK ansatz, whilst still employing the computational benefits of the Sobolev approximation in radiative transfer. In the MC-method, mass loss does not constitute an eigenvalue of the differential equations that govern the stellar wind, but the rates follow from assuming a wind velocity structure – in the form of a so-called $\beta$-law (Castor & Lamers 1979, CAK). The advantages of using the MC-method are manifold. There is no dependence on the CAK ansatz and the resulting CAK critical point, whilst the line acceleration is computed at all points in the wind without relying on a simplistic force multiplier approach involving a 2-parameter power-law approximation for the line acceleration. Furthermore, multiple scatterings can be included naturally

through Monte Carlo simulations. Because the kinetic energy density at the sonic point is negligible compared to that in the terminal flow, the MC-method does not rely on details of the trans-sonic flow (Lucy 2007a). Finally, the terminal wind velocity is a direct and accurate (within ∼10%) observable quantity in the local Universe.

It is probably for these reasons that the Vink et al. (2000) MC mass-loss rates[1] are widely used in evolutionary calculations, but however successful the MC approach may be in correctly predicting the mass-loss metallicity dependence (Vink et al. 2001; Mokiem et al. 2007b), the current MC approach is semi-empirical. Just as we are not able to obtain empirical mass-loss rates from the early Universe, neither will we be able to obtain direct wind velocities. It is therefore important that we develop a reliable theoretical framework through which we are able to predict the mass-loss rate and wind velocity simultaneously.

We first derive analytical solutions for the general velocity and density structure in any mass outflow or inflow situation. The solutions are obtained using the so-called Lambert $W$ function (Müller 2001; Cranmer 2004). As our solutions are presented in an explicit analytical form, physical insight can more easily be obtained through parameter changes. This in contrast to pure numerical models, where it is more challenging to predict the response of changes in the underlying parameters. For the specific case of a radiation-driven wind, we do not rely on the CAK expression for the radiation force, rather we describe the line acceleration as a function of stellar radius, $g(r)$. In addition, the critical point of our stellar wind is the sonic point (as in Parker 1958 solar wind theory), and not the CAK critical point. The calculation of $g(r)$ is performed through Monte Carlo simulations accounting for multi-line transfer, and the wind parameters are solved simultaneously in an iterative way.

The set-up of the paper is as follows. In Sects. 2.1–2.4, the hydrodynamic equations for a spherically symmetric steady flow are introduced including a derivation of the mathematical description of the radiative line acceleration as a function of radius for the case of a radiation-driven wind. The process for obtaining the fully analytical 1D solutions is described and discussed in Sect. 2.5. Here, the velocity field for the entire family of solutions is provided in an explicit general expression from which the solutions for a radiation-driven wind or mass accretion flux (e.g. collapsing protostellar cloud) follow as unique trans-sonic solutions through the critical point. Moreover, an approximate analytical solution for the supersonic flow is presented. In Sect. 3, we describe our numerical computation obtaining the radiative acceleration in our stellar wind models. Furthermore, a new iterative method for the determination of the consistent solution for the mass-loss rate is provided. In Sect. 4, we present the application of our models to the stellar wind from a typical O5-V-star, and discuss the results, before we summarise and discuss our findings in Sect. 5.

## 2. Radiation hydrodynamics of expanding or collapsing systems

### 2.1. Basic equations of hydrodynamics

Considering a non-viscous, i.e. ideal fluid, the momentum equation

$$\rho \frac{\mathrm{D}\boldsymbol{v}}{\mathrm{D}t} = \boldsymbol{f} - \boldsymbol{\nabla} p \tag{1}$$

is valid (see, e.g., Mihalas & Weibel Mihalas 1984), where $\mathrm{D}/\mathrm{D}t$ is the covariant Lagrangean or co-moving time derivative in the fluid-frame of a material element and $\boldsymbol{v}$ is its velocity, $\boldsymbol{f}$ is the total external body force per volume acting on a mass element of fluid, and $\boldsymbol{\nabla} p$ is the divergence term of a diagonal isotropic stress tensor $\boldsymbol{\nabla} \cdot \mathsf{T}$, in which $\mathsf{T} = -p\,\mathsf{I}$ and $p$ is the hydrostatic pressure.

One also needs to consider the equation of continuity

$$\frac{\partial \rho}{\partial t} + \boldsymbol{\nabla} \cdot (\rho\, \boldsymbol{v}) = 0, \tag{2}$$

with the covariant divergence $\boldsymbol{\nabla} \cdot \boldsymbol{v}$ of the velocity vector.

### 2.2. Simplifying assumptions

In order to solve the hydrodynamic equations analytically, and to account for the spherically symmetric stationary problem, we make the following simplifying assumptions:

1. The stellar wind is isothermal with a temperature equal to the effective temperature $T_{\rm eff}$ of the central star. In this case, the equation of state
$$p = a^2 \rho \tag{3}$$
is valid, where $a$ is the isothermal speed of sound and $\rho$ is the density of the wind.
2. We assume a stationary 1D spherical flow,
$$\frac{\partial}{\partial t} \equiv 0, \quad \frac{\partial}{\partial \phi} = \frac{\partial}{\partial \theta} \equiv 0, \quad f_\phi = f_\theta \equiv 0 \tag{4}$$
i.e. no shocks, no clumps, and no significant distortion of the star.
3. In the case of a wind from a luminous early-type star, the wind is primarily driven by continuum plus line radiation forces, where the radial acceleration on a mass element is
$$\frac{f_{\rm r}}{\rho} = -\frac{G\,M}{r^2}\,(1-\Gamma) + g_{\rm rad}^{\rm line} \tag{5}$$
with
$$\Gamma := \frac{g_{\rm rad}^{\rm cont}}{g}, \tag{6}$$
the force ratio between the radiative acceleration $g_{\rm rad}^{\rm cont}$ due to the continuum opacity (dominated by electron scattering) and the inward acceleration of gravity $g$. $\Gamma$ is supposed to be independent of radius $r$ and $g_{\rm rad}^{\rm line}(r)$ is the outward radiative acceleration due to spectral lines. $M$ is the mass of the central star.

### 2.3. Simplified hydrodynamic equations

#### 2.3.1. Wind density and mass-loss rate

If we use the covariant derivative (see Mihalas & Weibel Mihalas 1984) for spherical coordinates and apply assumption 2 to the equation of continuity (2), we find

$$\frac{\partial}{\partial r}\left(r^2\,\rho\, v\right) = 0 \tag{7}$$

for a one-dimensional, spherically symmetric and steady flow. Integrating this equation yields the conserved total mass flux (or

[1] http://star.arm.ac.uk/~jsv/

mass-loss rate) through a spherical shell with radius $r$ surrounding the star

$$\dot{M} = 4\,\pi\,r^2\,\rho\,(r)\,v\,(r) = \text{const.}, \tag{8}$$

or equivalently, for the wind density

$$\rho\,(r) = \frac{\dot{M}}{4\,\pi\,r^2\,v\,(r)} = \frac{F}{\hat{r}^2\,v\,(\hat{r})} \tag{9}$$

with the defined flux $F = \dot{M}\,/4\,\pi\,R^2$ through the star's surface at radius $R$ and the dimensionless radius $\hat{r} = (r/R)$.

Important note: all formulae derived in this Sect. 2 are expressed in terms of $\hat{r}$ referring to the radius $R$, which is (throughout this section) the stellar (i.e. photospheric) radius of the central star. However, all formulae can generally also be applied regarding the reference radius $R$ to be the inner boundary radius $R_{\rm in}$ (close to the stellar photosphere), from where the computations of a numerical wind model start (see, e.g., the results for an O-star in Sect. 4 and associated diagrams in this Sect. 2).

#### 2.3.2. The equation of motion

By using the correct contravariant components of acceleration $(\mathrm{D}\,v_i/\mathrm{D}\,t)$ in Eq. (1), for spherical coordinates, and replacing them by their equivalent physical components (see again, e.g., Mihalas & Weibel Mihalas 1984), and applying assumptions 1–3, we obtain the simplified $r$-component of the momentum equation of a spherically symmetric steady flow

$$\hat{v}\,\frac{\mathrm{d}}{\mathrm{d}\hat{r}}\,\hat{v} = -\frac{\hat{v}_{\rm crit}^2}{\hat{r}^2} + \hat{g}_{\rm rad}^{\rm line} - \frac{1}{\rho}\,\frac{\mathrm{d}\rho}{\mathrm{d}\hat{r}}, \tag{10}$$

in dimensionless form. The following dimensionless velocities (in units of the isothermal sound speed $a$)

$$\hat{v} := \frac{v}{a}, \quad \hat{v}_{\rm crit} := \frac{1}{a}\,\sqrt{\frac{GM}{R}\,(1-\Gamma)}, \tag{11}$$

and dimensionless line acceleration

$$\hat{g}_{\rm rad}^{\rm line} := \frac{R}{a^2}\,g_{\rm rad}^{\rm line} \tag{12}$$

are used. $v_{\rm crit}$ equals the rotational break-up velocity in the case of a corresponding rotating star, but here it is simply the effective escape velocity $v_{\rm esc}$ divided by a factor of $\sqrt{2}$

$$v_{\rm crit} \equiv \frac{v_{\rm esc}}{\sqrt{2}}.$$

By means of Eq. (9) and applying the chain rule to the function $1/v_{\rm r}(\hat{r})$, we obtain

$$\begin{aligned}\frac{\mathrm{d}\rho}{\mathrm{d}\hat{r}} &= \left(-\frac{2}{\hat{r}^3}\,\frac{1}{v\,(\hat{r})} - \frac{1}{\hat{r}^2}\,\frac{1}{v\,(\hat{r})^2}\,\frac{\mathrm{d}v\,(\hat{r})}{\mathrm{d}\hat{r}}\right) F \\ &\equiv -\rho\,(\hat{r})\,\left(\frac{2}{\hat{r}} + \frac{1}{v\,(\hat{r})}\,\frac{\mathrm{d}v\,(\hat{r})}{\mathrm{d}\hat{r}}\right).\end{aligned}$$

Using this expression for $\mathrm{d}\rho/\mathrm{d}\hat{r}$ in Eq. (10), we finally find the dimensionless differential *equation of motion* for the radial velocity

$$\left(\hat{v} - \frac{1}{\hat{v}}\right)\,\frac{\mathrm{d}}{\mathrm{d}\,\hat{r}}\,\hat{v} = -\frac{\hat{v}_{\rm crit}^2}{\hat{r}^2} + \frac{2}{\hat{r}} + \hat{g}_{\rm rad}^{\rm line}, \tag{13}$$

that is now independent of $\rho$.

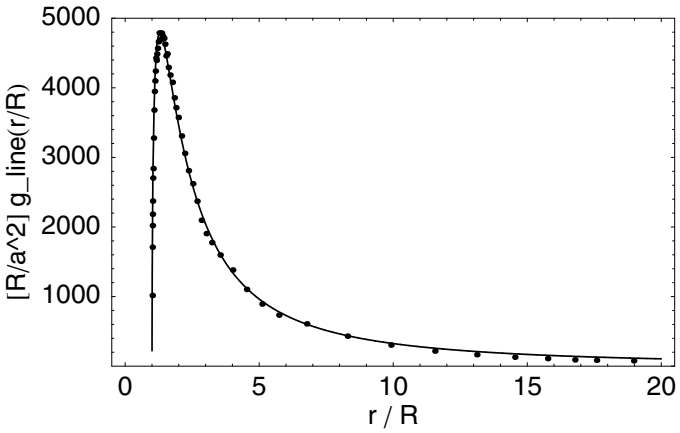


**Fig. 1.** The dimensionless radiative line acceleration $\hat{g}_{\rm rad}^{\rm line}\,(\hat{r})$ vs. radial distance $\hat{r}$ (in units of $R = 11.757\ R_\odot$) in the wind from a typical O5-V-star (see stellar parameters in Sect. 4). The dots represent the results from a numerical calculation of $\hat{g}_{\rm rad}^{\rm line}\,(\hat{r}_i)$ for discrete radial grid points $\hat{r}_i$. In order to determine the line acceleration parameters $\hat{g}_0$, $\gamma$, $\delta$ and $\hat{r}_0$ in Eq. (14), these values were fit to this non-linear model equation resulting in the displayed fitting curve (solid line) with the parameters $\hat{g}_0 = 17\,661$, $\gamma = 0.4758$, $\delta = 0.6878$ and $\hat{r}_0 = 1.0016$ (according to $v_\infty = 3232\ \mathrm{km\,s^{-1}}$), at the end of the iteration process (of type A), described in Sects. 3.3 and 4, respectively.

### *2.4. The line acceleration term and the final equation of motion*

To derive a sophisticated mathematical expression for the radiative line acceleration as a function of radius $r$ only, we collect all the physically motivated mathematical properties of this function $\hat{g}_{\rm rad}^{\rm line}\,(\hat{r})$:

1. For hydrostatic reasons, $\hat{g}_{\rm rad}^{\rm line}$ should be zero at a particular radius $\hat{r}'(\approx 1)$ near the stellar photosphere:

   $$\hat{g}_{\rm rad}^{\rm line}\,(\hat{r} = \hat{r}') = 0,$$

2. $\hat{g}_{\rm rad}^{\rm line}$ should always be positive (except close to the stellar surface, see item 1) as the radiation from the photosphere is streaming outwards and so is the radiative force:

   $$\hat{g}_{\rm rad}^{\rm line}\,(\hat{r}) > 0 \quad \text{for} \quad \hat{r} > \hat{r}',$$

3. $\hat{g}_{\rm rad}^{\rm line}$ is supposed to decrease (i.e. goes to zero) as $1/\hat{r}^2$ (cf. Castor 1974; Abbott 1980) with increasing radial distance $\hat{r}$ from the central star:

   $$\hat{g}_{\rm rad}^{\rm line}\,(\hat{r}) \approx \frac{1}{\hat{r}^2} \longrightarrow 0 \quad \text{for} \quad \hat{r} \longrightarrow \infty,$$

4. $\hat{g}_{\rm rad}^{\rm line}$ has an absolute maximum somewhere in the range between the stellar surface and the outer edge of the wind because of the properties 1–3 above:

   $$0 \le \hat{g}_{\rm rad}^{\rm line}\,(\hat{r}) \le \hat{g}_{\rm rad}^{\rm line}\,(\hat{r}_{\rm max}).$$

All these mathematical properties for the radiative line acceleration term can be realised by the function

$$\hat{g}_{\rm rad}^{\rm line}(\hat{r}) = \frac{\hat{g}_0}{\hat{r}^{1+\delta}}\,\left(1 - \frac{\hat{r}_0}{\hat{r}^\delta}\right)^\gamma \tag{14}$$

or equivalently,

$$\hat{g}_{\rm rad}^{\rm line}(\hat{r}) = \frac{\hat{g}_0}{\hat{r}^{1+\delta\,(1+\gamma)}}\,\left(\hat{r}^\delta - \hat{r}_0\right)^\gamma, \tag{15}$$

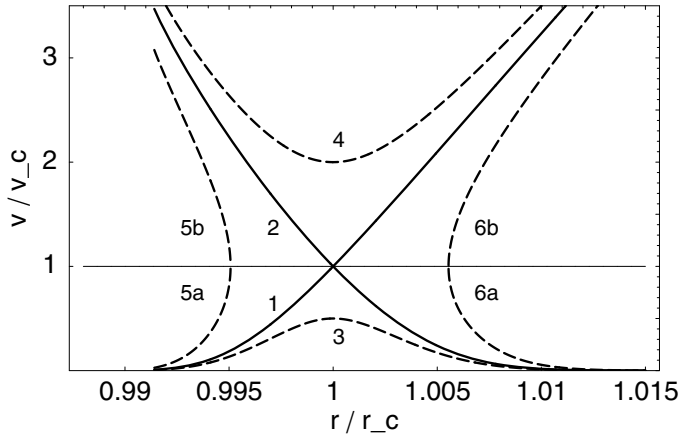


**Fig. 2.** The topology of solutions $|v(\hat{r}/\hat{r}_c)/a|$ of the equation of motion, Eq. (16), vs. radial distance in units of the critical radius $\hat{r}_c$, for a typical O5-V-star in the centre with the line acceleration parameters $\hat{g}_0 = 17661$, $\gamma = 0.4758$, $\delta = 0.6878$ and $\hat{r}_0 = 1.0016$ in Eq. (14), according to $v_\infty = 3232$ km s$^{-1}$ (see further stellar parameters in Sect. 4). The horizontal line marks the critical velocity (i.e. sound speed $v_c = a$). Solution 1 is the unique trans-sonic stellar wind solution through the critical point at $\hat{r}_c = \hat{r}_s = 1.0110$ and $\hat{v}(\hat{r}_c) = 1.0$. For the description of the different solutions of type 2–6, see the discussion in Sects. 2.5.1 and 2.5.4.

which is independent of $\hat{v}$ and $(\mathrm{d}\hat{v}/\mathrm{d}\hat{r})$, and is a function of $\hat{r}$ only.

We note that the position of the maximum $(\hat{r}_{\max}, \hat{g}^{\rm line}_{\rm rad}(\hat{r}_{\max}))$ has to be variable and adjustable for each set of stellar and wind parameters, as the number and species of spectral lines that make up the radial force are also variable with each stellar wind. We therefore had to introduce the two parameters, $\hat{g}_0$ and $\gamma$. Moreover, item 1 is fulfilled at radius $\hat{r}' = \hat{r}_0^{1/\delta}$ and item 3 can be guaranteed by appropriate values of the exponents $\delta$ and $\gamma$ (where $0 < \gamma \lesssim 1$ and $0 < \delta \lesssim 1$). Altogether, we had to introduce at least the set of four parameters in Eqs. (14) and (15).

Thus, the equation of motion (13) becomes

$$\left(\hat{v} - \frac{1}{\hat{v}}\right) \frac{\mathrm{d}}{\mathrm{d}\hat{r}}\,\hat{v} = -\frac{\hat{v}^2_{\rm crit}}{\hat{r}^2} + \frac{2}{\hat{r}} + \frac{\hat{g}_0}{\hat{r}^{1+\delta\,(1+\gamma)}} \left(\hat{r}^\delta - \hat{r}_0\right)^\gamma . \tag{16}$$

This equation is fully solvable analytically as we show later.

### 2.5. Analytical solutions of the equation of motion

#### 2.5.1. The critical point and critical solutions

The equation of motion (Eqs. (13) and (16)) yields several families of solutions that have quite different mathematical behaviour and physical significance (cf. Fig. 2).

The left hand side of Eq. (16) vanishes for $(\mathrm{d}\hat{v}/\mathrm{d}\hat{r} \neq 0)_{\hat{r}_c}$ at the critical radius $\hat{r}_c$, where

$$\hat{v}\,(\hat{r}_c) \equiv \hat{v}\,(\hat{r}_s) = 1. \tag{17}$$

That is, the critical point velocity here is equal to the isothermal sound speed $\hat{v} = 1$, and the critical radius is just the sonic radius

$$\hat{r}_c \equiv \hat{r}_s,$$

as is also the case for thermal winds or mass accretion events (where $\hat{g}^{\rm line}_{\rm rad} \approx 0$).

We are now interested in under what conditions one can obtain a continuous and smooth trans-sonic flow through the critical point $\hat{r}_c$ of Eq. (16). For the case of a stellar wind, this means how to obtain a smooth transition from subsonic and subcritical flow ($\hat{v} < \hat{v}_c = 1$) at small $\hat{r} < \hat{r}_c$ to supercritical and supersonic flow ($\hat{v} > \hat{v}_c$) at large $\hat{r} > \hat{r}_c$, when this critical solution has a finite positive slope $(\mathrm{d}\hat{v}/\mathrm{d}\hat{r}) > 0$ at $\hat{r} = \hat{r}_c$ (cf. solid curve 1 in Fig. 2)[2]? Then, it is evident from the left hand side of Eq. (16) that one can obtain such a trans-sonic wind, if the right hand side (1) vanishes at the critical radius $\hat{r}_c$, (2) is negative for $\hat{r} < \hat{r}_c$, and (3) is positive for $\hat{r} > \hat{r}_c$.

The opposite situation occurs for the case of mass accretion in e.g. a collapsing cloud. If $(\mathrm{d}\hat{v}/\mathrm{d}\hat{r})_{\hat{r}_c} < 0$, we obtain the second unique trans-sonic and critical solution in which $\hat{v}\,(\hat{r})$ is monotonically decreasing from supersonic speeds for $\hat{r} < \hat{r}_s$, e.g. near the protostar, to subsonic speeds for $\hat{r} > \hat{r}_s$ at the outer edge of the cloud (see also the second solid line 2, in Fig. 2, for the case of a corresponding accretion flow with a star as the central object).

Here we are mainly interested in the critical *wind* solution of Eq. (16). The right hand side of Eq. (16) vanishes at the critical radius $\hat{r}_c$ that solves the equation

$$2\,\hat{r}^{\delta\,(1+\gamma)} - \hat{v}^2_{\rm crit}\,\hat{r}^{\delta\,(1+\gamma)-1} + \hat{g}_0 \left(\hat{r}^\delta - \hat{r}_0\right)^\gamma = 0. \tag{18}$$

Therefore, the critical radius has to be determined numerically by means of the above equation and the line term parameters $\hat{g}_0$, $\gamma$, $\delta$ and $\hat{r}_0$. However, if one assumes values of $\gamma$ and $\delta$ close to 1, one can provide a good approximation (i.e. analytical solution of Eq. (18)) for the critical radius

$$\hat{r}_c \approx \frac{\left(\hat{v}^2_{\rm crit} - \hat{g}_0\right) + \sqrt{\left(\hat{v}^2_{\rm crit} - \hat{g}_0\right)^2 + 8\,\hat{g}_0\,\hat{r}_0}}{4}\,. \tag{19}$$

For the special case of a thermal wind, where $\hat{g}_0$ can be set to zero, we obtain

$$\hat{r}_c = \hat{r}_s = \frac{\hat{v}^2_{\rm crit}}{2} = \frac{G\,M\,(1-\Gamma)}{2aR}\,. \tag{20}$$

In some special cases of mass accretion (e.g. a collapsing cloud), one can even set $\Gamma = 0$.

#### 2.5.2. Solving the equation of motion

The Equation of motion (16) can be solved by first integrating the lefthand side over $\hat{v}$, and then integrating the righthand side over $\hat{r}$, separately, which yields

$$\hat{v}^2 - \ln \hat{v}^2 = 2\frac{\hat{v}^2_{\rm crit}}{\hat{r}} + 4\,\ln \hat{r} + \frac{2}{\hat{r}_0}\,\frac{\hat{g}_0}{\delta\,(1+\gamma)} \left(1 - \frac{\hat{r}_0}{\hat{r}^\delta}\right)^{1+\gamma} + C, \tag{21}$$

with the right hand side of Eq. (21) denoted as the function

$$f\,(\hat{r};\hat{r}',\hat{v}') := 2\frac{\hat{v}^2_{\rm crit}}{\hat{r}} + 4\,\ln \hat{r} + \frac{2}{\hat{r}_0}\,\frac{\hat{g}_0}{\delta\,(1+\gamma)} \left(1 - \frac{\hat{r}_0}{\hat{r}^\delta}\right)^{1+\gamma} + C(\hat{r}',\hat{v}') \tag{22}$$

with the constant of integration $C$ that is determined by the boundary condition of the radial velocity $\hat{v}'$ at a given radius $\hat{r}'$.

From Eq. (21), we can determine $C\,(\hat{r}',\hat{v}')$ for the solution that passes through the particular point $(\hat{r}',\hat{v}')$,

$$C\,(\hat{r}',\hat{v}') = \hat{v}'^2 - \ln \hat{v}'^2 - 2\frac{\hat{v}^2_{\rm crit}}{\hat{r}'} - 4\,\ln \hat{r}' - \frac{2}{\hat{r}_0}\,\frac{\hat{g}_0}{\delta\,(1+\gamma)} \left(1 - \frac{\hat{r}_0}{\hat{r}'^\delta}\right)^{1+\gamma}. \tag{23}$$

[2] We furthermore assume that both $\hat{v}$ and $(\mathrm{d}\hat{v}/\mathrm{d}\hat{r})$ are *everywhere* single-valued and continuous.

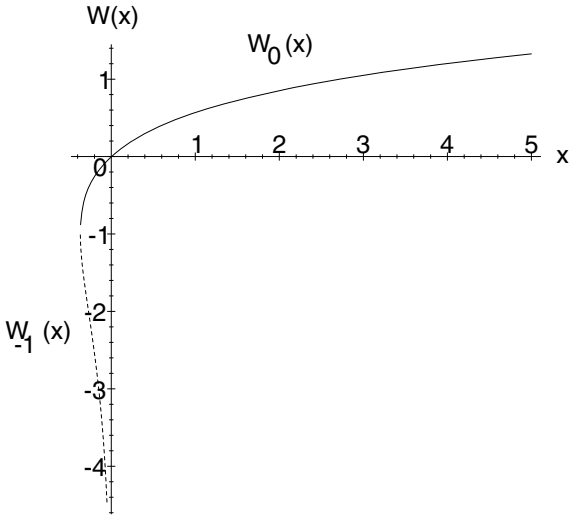


**Fig. 3.** The two real branches of the Lambert $W$ function: $W_0(x)$ (full curve) and $W_{-1}(x)$ (broken curve).

Therefore the function $f$ in Eq. (22) becomes

$$f(\hat{r};\hat{r}',\hat{v}') = \hat{v}'^2 - \ln \hat{v}'^2 + 2\,\hat{v}_{\rm crit}^2\left(\frac{1}{\hat{r}} - \frac{1}{\hat{r}'}\right) + 4\,\ln\left(\frac{\hat{r}}{\hat{r}'}\right) + \frac{2}{\hat{r}_0}\,\frac{\hat{g}_0}{\delta\,(1+\gamma)}\left[\left(1-\frac{\hat{r}_0}{\hat{r}^{\delta}}\right)^{1+\gamma} - \left(1-\frac{\hat{r}_0}{\hat{r}'^{\delta}}\right)^{1+\gamma}\right]. \quad (24)$$

And from this, Eq. (21) now reads

$$\hat{v}^2 - \ln \hat{v}^2 = f(\hat{r};\hat{r}',\hat{v}')$$

or, equivalently,

$$-\,\hat{v}^2\,{\rm e}^{-\hat{v}^2} = -{\rm e}^{-f(\hat{r};\hat{r}',\hat{v}')}, \quad (25)$$

which is solved explicitly and fully analytically in terms of the Lambert $W$ function.

### 2.5.3. The Lambert $W$ function

The $W$ function is defined to be the implicit function satisfying

$$W(z)\,{\rm e}^{W(z)} = z \quad (26)$$

(cf. Corless et al. 1993, 1996).

As the equation $y(x)\exp y(x) = x$ has an infinite number of solutions $y(x)$ for each non-zero value of $x$, $W$ has an infinite number of branches. We are only interested in the physically relevant case, where $x$ is real and $-1/e \le x < 0$. Then, there are two possible real values of $W(x)$ (see Fig. 3). As one can already see from the defining equation of $W$, the $W$ function vanishes at $x = 0$, is negative for $x < 0$, positive for positive values of $x$, and must be $-1$ at the point $x = -1/e$. The branch satisfying $-1 \le W(x)$ for $x$ in the range of $[-1/e, \infty)$ is denoted by $W_0(x)$ or just $W(x)$, and the branch satisfying $W(x) \le -1$ over the interval $[-1/e, 0)$ by $W_{-1}(x)$. The branches $W_0(x)$ and $W_{-1}(x)$ share the branch point at $x = -1/e$. $W_0(x)$ is referred to as the *principal branch* of the $W$ function, which is the only branch that is analytic at 0. The other remaining non-principal branches of $W$ all have a branch point at 0, and they are denoted by $W_k(x)$, where $k$ is a non-zero integer.

### 2.5.4. The solution(s) of the equation of motion

It is now possible to provide an explicit analytical expression for the solution $\hat{v}$ of the equation of motion (16), or Eq. (25), by means of the $W$ function. If we compare Eq. (25) with the defining equation of the Lambert $W$ function (Eq. 26),

$$W_k(x)\,{\rm e}^{W_k(x)} = x,$$

we find that

$$-\hat{v}^2 = W_k(x)$$

or

$$\hat{v} = \pm\sqrt{-W_k(x)} \quad (27)$$

is the *general solution* of the equation of motion that passes through the point $(\hat{r}', \hat{v}')$, with the argument function of the $W$ function

$$x(\hat{r}) = -{\rm e}^{-f(\hat{r};\hat{r}',\hat{v}')}. \quad (28)$$

Since the argument of the $W$ function in Eq. (27) is always real and negative, it is guaranteed that the argument of the square root never becomes negative, and hence the solution is always real (see Fig. 3).

Inserting $f(\hat{r};\hat{r}',\hat{v}')$ from Eqs. (24) into (28) yields

$$x(\hat{r};\hat{r}',\hat{v}') = -\left(\frac{\hat{r}'}{\hat{r}}\right)^4 \hat{v}'^2\,\exp\left[-2\,\hat{v}_{\rm crit}^2\left(\frac{1}{\hat{r}} - \frac{1}{\hat{r}'}\right) - \frac{2}{\hat{r}_0}\,\frac{\hat{g}_0}{\delta\,(1+\gamma)}\left(\left(1-\frac{\hat{r}_0}{\hat{r}^{\delta}}\right)^{1+\gamma} - \left(1-\frac{\hat{r}_0}{\hat{r}'^{\delta}}\right)^{1+\gamma}\right) - \hat{v}'^2\right], \quad (29)$$

the general expression for the argument function $x$ depending on the parameters $(\hat{r}', \hat{v}')$.

Thus, for the *trans-sonic* case of a *stellar wind* or general *accretion flow*, where $\hat{r}' = \hat{r}_{\rm c} \equiv \hat{r}_{\rm s}$ and $\hat{v}' = \hat{v}_{\rm c} \equiv 1$, the analytical solution is

$$\hat{v}(\hat{r}) = \pm\sqrt{-W_k(x(\hat{r}))} \quad (30)$$

with

$$x(\hat{r}) = -\left(\frac{\hat{r}_{\rm c}}{\hat{r}}\right)^4 \exp\left[-2\,\hat{v}_{\rm crit}^2\left(\frac{1}{\hat{r}} - \frac{1}{\hat{r}_{\rm c}}\right) - \frac{2}{\hat{r}_0}\,\frac{\hat{g}_0}{\delta\,(1+\gamma)}\left(\left(1-\frac{\hat{r}_0}{\hat{r}^{\delta}}\right)^{1+\gamma} - \left(1-\frac{\hat{r}_0}{\hat{r}_{\rm c}^{\delta}}\right)^{1+\gamma}\right) - 1\right]. \quad (31)$$

From this equation, one can easily derive the solution for the simpler cases of a *thermal wind* (e.g. the solar wind), or for a particular *accretion flow*, as e.g. a collapsing molecular cloud, where $\hat{g}_0$ can be set to zero and $\hat{v}_{\rm crit}^2 = 2\,\hat{r}_{\rm c}$ (cf. Eq. (20)):

$$\hat{v}(\hat{r}) = \pm\sqrt{-W_k\left(-\left(\frac{\hat{r}_{\rm c}}{\hat{r}}\right)^4 \exp\left(3 - 4\,\frac{\hat{r}_{\rm c}}{\hat{r}}\right)\right)}. \quad (32)$$

Here, the minus sign (in front of the square root) refers to the collapsing system.

We are only interested in the possible two real values of $W(x)$, the $k = 0, -1$ – branches in Eqs. (27) or (30), where $x$ is real and $-1/e \le x < 0$. The branch point at $x = -1/e$, where these two branches meet, corresponds to the critical point $\hat{r}_{\rm c}$, where the velocity in Eq. (30) becomes $\hat{v} = \hat{v}(\hat{r}_{\rm c}) \equiv 1$. Depending on which branch of $W$ one is approaching this point $x = -1/e$,

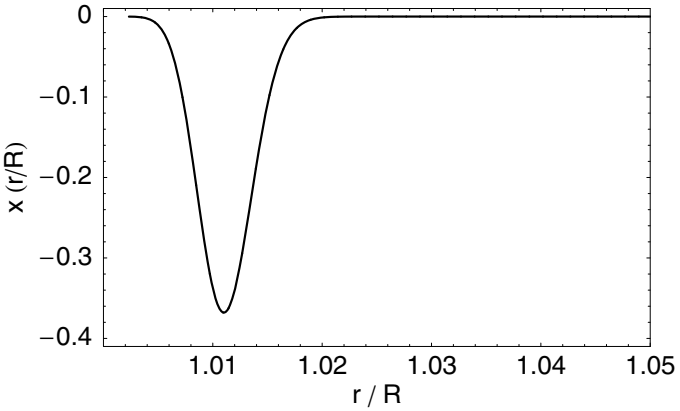


**Fig. 4.** The argument function $x(\hat{r})$ of the $W$ function, Eq. (31), in the trans-sonic velocity law, Eq. (30), vs. radial distance $\hat{r} = r/R$ for the stellar wind from a typical O5-V-star with the line acceleration parameters $\hat{g}_0 = 17661$, $\gamma = 0.4758$, $\delta = 0.6878$ and $\hat{r}_0 = 1.0016$ in Eq. (14), according to $v_\infty = 3232$ km s$^{-1}$ (see further stellar parameters in Sect. 4). The minimum of this function is at the critical radius $\hat{r}_c = \hat{r}_s = 1.0110$ where $x(\hat{r}_c) = -1/e$.

one obtains a different shape of the $\hat{v}(\hat{r})$-curve, i.e. a stellar wind or a collapsing system.

However, to determine which of the two branches to choose at a certain range of radius between $[1, \hat{r}_c]$ and $[\hat{r}_c, \infty)$ so as to guarantee a continuous, monotonically increasing, and smooth trans-sonic flow (as in the case of a wind), one still needs to examine the behaviour of the argument function $x(\hat{r})$ of $W$, in Eq. (31), with radius $\hat{r}$ (see Fig. 4).

The argument function $x(\hat{r})$ decreases monotonically from the stellar radius $\hat{r} = 1$ (with a value of nearly zero) to its minimum at $\hat{r} = \hat{r}_c$ with $x = -1/e$ to afterwards increase monotonically again.

STELLAR WIND: by choosing first the real principal branch $W_0(x)$ of the Lambert function that is followed in the negative direction until the critical point $x(\hat{r}_c) = -1/e$ and $W_0(x) = -1$ (i.e. $\hat{v}(\hat{r}_c)$) for rising radii from near the star surface $\hat{r} \approx 1$, and hence coming from $x(\hat{r}) \lesssim 0$ and $W_0(x) \lesssim 0$, yields the desired critical wind solution. This choice causes the strict monotonic increase of the velocity $\hat{v}(\hat{r})$ from nearly zero until the sonic point (in the subsonic region). To ensure that the solution passes smoothly through this critical point, i.e. that the derivative $\hat{v}'(\hat{r}_c)$ is continuous, one has to change there to the $W_{-1}(x)$-branch. From there onwards, the real part of this branch is followed further in the negative direction $W_{-1}(x) \to -\infty$ for larger radii and therefore with decreasing $|x(\hat{r})| \to 0$, again. From this, one obtains the desired continued monotonic slope of $\hat{v}(\hat{r})$ in the supersonic region for $\hat{r} > \hat{r}_c (= \hat{r}_s)$.

ACCRETION SOLUTION: in this case, the unique critical and trans-sonic solution $|\hat{v}(\hat{r})|$ is strictly monotonically increasing from small values in the subsonic region far away from the central object (for $\hat{r} > \hat{r}_s$ and $|\hat{v}(\hat{r})| \ll 1$), into the supersonic region (for $\hat{r} < \hat{r}_s$ and $|\hat{v}(\hat{r})| > 1$) with declining radius $\hat{r}$. Here the slope $\hat{v}'$ is negative and continuous at the sonic (critical) radius $\hat{r}_s$ (as a necessary boundary condition). This case can be achieved when we again first take the $W_0(x)$-branch for $0 \geq x(\hat{r}) \geq -1/e$ (in the subsonic region) and then change over at the sonic point to the $W_{-1}(x)$-branch for $-1/e \leq x(\hat{r}) < 0$; now however with decreasing radius $\hat{r} \to 1$. Here one is again wandering in the same negative direction through the possible two real values of $W(x)$ in the range of $-1/e \leq x < 0$. We are approaching the critical point $x(\hat{r}_s) = -1/e$ (where the argument function $x(\hat{r})$ has its minimum, cf. Fig. 4) with declining radii $\hat{r} > \hat{r}_s$ from the right side and from $x(\hat{r}) \lesssim 0$, in order to change the branch at this point, where $x(\hat{r})$ afterwards increases again strictly monotonically (with smaller radii) until almost $x(\hat{r}_\star) \lesssim 0$ near the central object.

To summarise, the velocity in the radial direction (i.e. the exact analytical and spherically trans-sonic solution of our equation of motion) can be described,

(a) for the case of a *stellar wind*, by Eq. (30) (and the positive sign in front of the root) and the argument function in Eq. (31), choosing the branch

$$k = \begin{cases} 0 & \text{for } 1 \leq \hat{r} \leq \hat{r}_c \\ -1 & \text{for } \hat{r} > \hat{r}_c \end{cases} \tag{33}$$

of the $W$ function at a certain radius $\hat{r}$, and

(b) in case of a *general accretion flux*, as well, by Eq. (30) (but now with the negative sign in front of the root) and the argument function in Eq. (31), choosing the branch

$$k = \begin{cases} -1 & \text{for } 1 \leq \hat{r} \leq \hat{r}_c \\ 0 & \text{for } \hat{r} > \hat{r}_c \end{cases} \tag{34}$$

depending on the location $\hat{r}$, and

(c) in the special cases of a *thermal wind or* collapsing system like a *collapsing protostellar cloud*, by Eq. (32), choosing the same branches as mentioned above in case (a), or (b) respectively, and the appropriate sign (in front of the root).

In addition to these two critical solutions (type 1 and 2, cf. numbering in Fig. 2), already discussed, that pass through the critical point (i.e. sonic point), all the other four types of solutions were obtained from our *general velocity law*, Eqs. (27) with (29), choosing the following branches of the $W$ function and values of $(\hat{r}', \hat{v}')$, for the point we demand the solution to go through:

- type-3: *subsonic (subcritical) solutions*

  $k = 0, \quad \hat{r}' = \hat{r}_c, \quad \hat{v}' < 1$

- type-4: *supersonic (supercritical) solutions*

  $k = -1, \quad \hat{r}' = \hat{r}_c, \quad \hat{v}' > 1$

- type-5 and 6: *double-valued solutions*

  $k = 0 \quad \text{and} \quad k = -1 \quad \text{for}$

  $\hat{r}', \hat{v}' = \text{arbitrarily, where} \quad \hat{r}' \neq \hat{r}_c, \quad \hat{v}' \neq 1.$

Type-3 solutions are everywhere subsonic (choosing only the principal branch, $k = 0$, of the $W$ function). Those of type 4 are everywhere supersonic (selecting only the $k = -1$-branch in the velocity law), and those of type 5 and 6 are double-valued, composed of both the $k = 0$ and $k = -1$-branch, below and above the sonic line, respectively. In this connection, the two sub- and supersonic pairs of curves of this last mentioned types, subdivided into (5a, 6a) and (5b, 6b) in Fig. 2, belong together. They are fixed, not only by the same chosen branch of $W$ in Eq. (27), but also by the same selected parameters for the solution through the identical given point $(\hat{r}', \hat{v}')$.

From our analytical wind solution, we find that $\hat{v}$ increases without limit as $\hat{r} \to \infty$. This unphysical increase in $\hat{v}$ at large $\hat{r}$ is an artificial consequence of our assumption (1) that the stellar wind is isothermal with a temperature, $T_{\text{eff}}$, of the central stellar photosphere. This assumption is valid close to the photosphere, but may not hold at large distances, where the gas expansion will

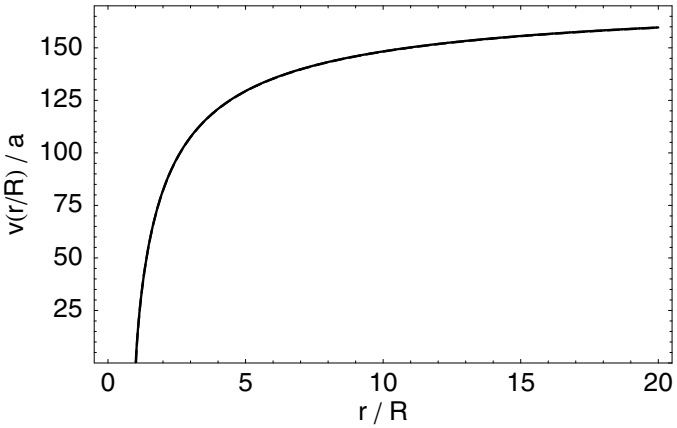


**Fig. 5.** Comparison of the approximated wind solution (invisible dashed line, overlaid by the solid line) with the exact solution $\hat{v}(\hat{r})$ (in units of sound speed) vs. radial distance $\hat{r}$ (in units of $R = 11.757\ R_\odot$) for the wind from a typical O5-V-star with the line acceleration parameters $\hat{g}_0 = 17\,661$, $\gamma = 0.4758$, $\delta = 0.6878$ and $\hat{r}_0 = 1.0016$ in Eq. (14), according to $v_\infty = 3232\ \mathrm{km\,s^{-1}}$ (see stellar parameters in Sect. 4). The approximated curve was obtained from Eq. (39), where the exact solution was obtained from Eq. (30), together with Eqs. (31) and (33), with a critical radius of $\hat{r}_c = 1.0110$. For a more detailed comparison see Fig. 7.

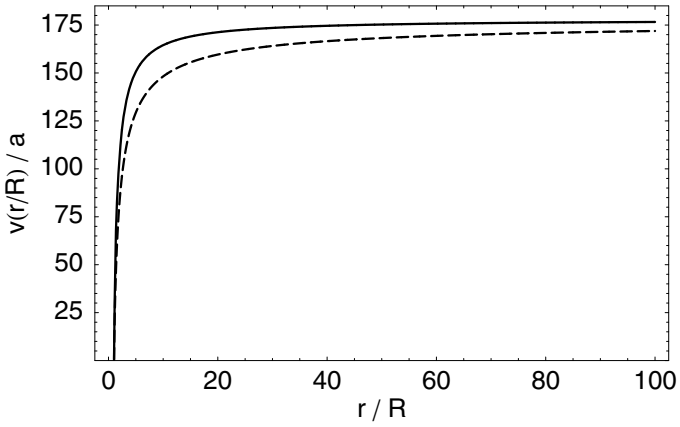


**Fig. 6.** Comparison of the approximated wind solution (dashed line) with the $\beta$ wind velocity law (solid line) $\hat{v}(\hat{r})$ (in units of sound speed $a$) over a large radial distance $\hat{r}$ (in units of $R = 11.757\ R_\odot$) for the wind from a typical O5-V-star. The approximated wind curve was obtained with the same parameters as in Fig. 5, where the $\beta$ wind velocity curve was retrieved from Eq. (41) with an exponent of $\beta = 0.7379$, a terminal velocity of $(v_\infty/a) = 177.9$ (according to $v_\infty = 3232\ \mathrm{km\,s^{-1}}$) and a parameter value of $\hat{r}_0' = 1.0095$ (used in ISA-Wind). Both curves approach the same velocity limit $v_\infty$ as $\hat{r}$ goes to infinity.

ultimately force the wind to cool down. By insisting on keeping the wind temperature $T$ fixed, we introduce an undesirable energy source to do work on the gas and accelerate it without limit. In the case of the solar wind, this classical problem was overcome in the work of Parker (1958; see also the review of Mihalas 1978) by assuming the corona near the sun to be isothermal, yet allowing the wind to expand adiabatically at larger radii.

We overcome this problem by deriving an analytical expression for the wind solution in the supersonic approximation, in the following Sect. 2.5.5, by neglecting the pressure term in the equation of motion which introduces a terminal velocity $v_\infty$, as well as a relationship between $v_\infty$ and our wind (and line acceleration) parameters $\hat{g}_0$, $\gamma$, $\delta$ and $\hat{r}_0$.

At the end of the iteration process (described in Sect. 3.3), we obtain the converged values of the previously mentioned wind model parameters, together with the real position of the critical radius $\hat{r}_c$, to be able to evaluate the final wind solution with Eqs. (30) and (31). This way, the complete (exact) wind velocity curve is produced (in Fig. 5) to be compared with the approximated wind solution over a wide wind range from the stellar photosphere up to a distance of 20 stellar radii. This comparison (see also the enlarged images of Fig. 7) shows a high level of agreement, and only a weak discrepancy between both curves $\hat{v}(\hat{r})$, in particular for larger radii, where the (even) unlimited function for the exact wind solution is close to the "speed" limited approximated solution curve. Through this way of adjustment, the undesirable unlimited mathematical behaviour of our expression for the wind velocity has become insignificant over the whole $\hat{r}$ range of interest.

The subsequently derived approximated wind solution is only valid in the supersonic region and is not supposed to be applied to the subsonic region, where it even becomes imaginary, particularly in our wind model in the range of $0 < \hat{r} \lesssim \hat{r}_s$, see upper diagram of Fig. 7. This explains the only noticeable discrepancy between both wind velocity curves in that radial range, from close above the sonic radius down to the stellar surface.

The numerically computed model atmospheres that we apply later in our iteration process allow a temperature stratification $T(r)$ of the wind, i.e. we do not assume a fixed $T$ as in our analytical expressions.

### 2.5.5. Approximated solution of the equation of motion

By neglecting the pressure term in the equation of motion (10),

$$\frac{1}{\rho}\frac{\mathrm{d}\rho}{\mathrm{d}\hat{r}} \approx 0,$$

which is a good approximation for the stellar wind solution in the supersonic region with $\hat{r} > \hat{r}_c \equiv \hat{r}_s$, Eq. (16) becomes

$$\hat{v}\,\frac{\mathrm{d}}{\mathrm{d}\,\hat{r}}\,\hat{v} = -\frac{\hat{v}_{\mathrm{crit}}^2}{\hat{r}^2} + \frac{\hat{g}_0}{\hat{r}^{1+\delta\,(1+\gamma)}}\,\left(\hat{r}^\delta - \hat{r}_0\right)^\gamma . \tag{35}$$

This simplified equation of motion can again be solved by first integrating the left hand side over $\hat{v}$, and then integrating the right hand side over $\hat{r}$, separately, which yields

$$\hat{v}^2 = 2\frac{\hat{v}_{\mathrm{crit}}^2}{\hat{r}} + \frac{2}{\hat{r}_0}\,\frac{\hat{g}_0}{\delta\,(1+\gamma)}\left(1 - \frac{\hat{r}_0}{\hat{r}^\delta}\right)^{1+\gamma} + C. \tag{36}$$

In order to determine the integration constant $C$, we assume a boundary condition $\hat{v}(\hat{r}') \approx 0$ for the wind velocity at radius $\hat{r}' = \hat{r}_0^{1/\delta}$, close to the stellar photosphere, i.e.

$$C\,(\hat{r}' = \hat{r}_0^{1/\delta}, \hat{v}' = 0) = -2\,\frac{\hat{v}_{\mathrm{crit}}^2}{\hat{r}_0^{1/\delta}}\,. \tag{37}$$

Thus, Eq. (36) now reads

$$\hat{v}^2 = 2\left(\hat{v}_{\mathrm{crit}}^2\left(\frac{1}{\hat{r}} - \frac{1}{\hat{r}_0^{1/\delta}}\right) + \frac{\hat{g}_0}{\hat{r}_0\,\delta\,(1+\gamma)}\left(1 - \frac{\hat{r}_0}{\hat{r}^\delta}\right)^{1+\gamma}\right), \tag{38}$$

resulting in the *approximated wind solution*

$$\hat{v}\,(\hat{r}) = \sqrt{\frac{2}{\hat{r}_0}\left(\hat{v}_{\mathrm{crit}}^2\left(\frac{\hat{r}_0}{\hat{r}} - \hat{r}_0^{1-1/\delta}\right) + \frac{\hat{g}_0}{\delta\,(1+\gamma)}\left(1 - \frac{\hat{r}_0}{\hat{r}^\delta}\right)^{1+\gamma}\right)}, \tag{39}$$

which can be expressed without the $W$ function.

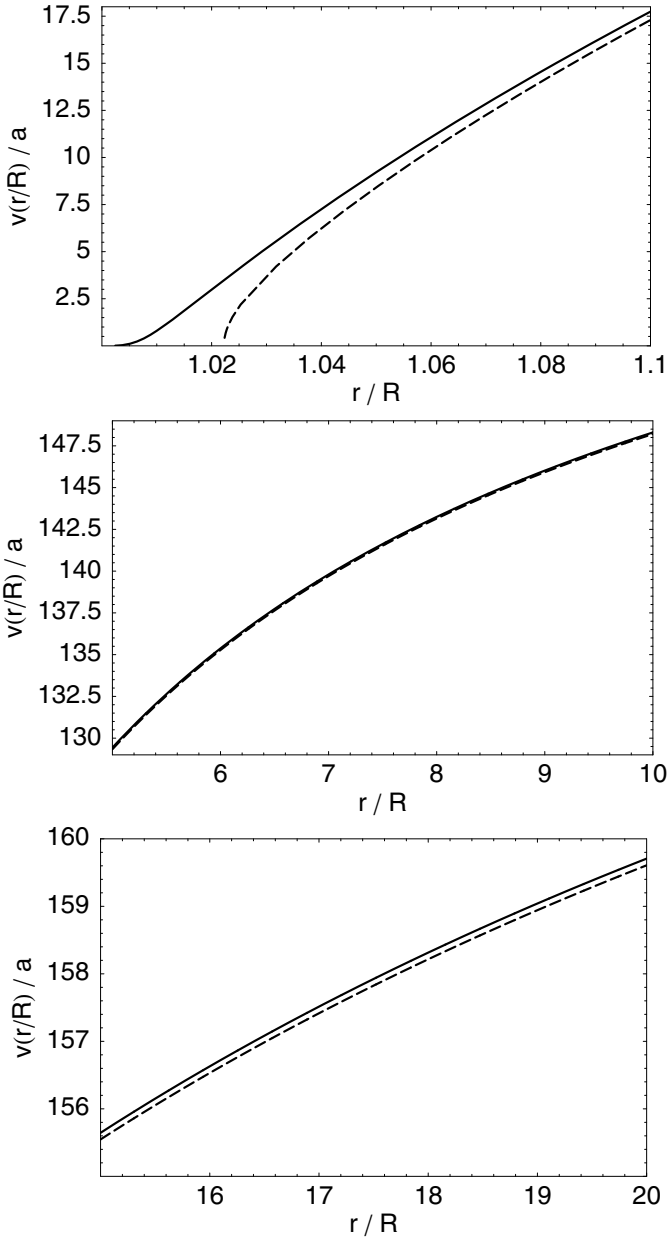


**Fig. 7.** Model results for the wind velocity $\hat{v}(\hat{r})$ (in units of sound speed $a$) vs. radial distance $\hat{r}$ (in units of $R = 11.757\ R_\odot$) from a typical O5-V-star with the line acceleration parameters $\hat{g}_0 = 17661$, $\gamma = 0.4758$, $\delta = 0.6878$ and $\hat{r}_0 = 1.0016$ (cf. Eq. (14)), and a critical radius of $\hat{r}_c = \hat{r}_s = 1.0110$ (see stellar parameters in Sect. 4). The approximated (dashed line) and the exact wind solution (solid line) are compared with each other for three different and magnified radial ranges: very close to the central star between $\hat{r} = [1.0, 1.1]$ (see upper diagram), at intermediate distance of $\hat{r} = [5.0, 10.0]$ (see middle diagram) and far away between $\hat{r} = [15.0, 20.0]$ (see lower diagram).

### 2.5.6. Comparison with the $\beta$ velocity law

Equation (39) yields a terminal velocity $\hat{v}_\infty$ (as $\hat{r} \to \infty$) of

$$\hat{v}_\infty = \sqrt{\frac{2}{\hat{r}_0}\left(\frac{\hat{g}_0}{\delta\,(1+\gamma)} - \hat{v}_{\rm crit}^2\,\hat{r}_0^{1-1/\delta}\right)}, \tag{40}$$

which is now comparable to the $\hat{v}_\infty$ parameter in a (so-called) $\beta$ velocity law (cf. Castor & Lamers 1979, CAK)

$$\hat{v}\,(\hat{r}) = \hat{v}_\infty\left(1 - \frac{\hat{r}_0'}{\hat{r}}\right)^\beta. \tag{41}$$

To be able to compare the $\gamma$ (and $\delta$) parameter in our wind law with the exponent in the $\beta$ law (as we use $\beta$ as an input parameter in our model atmosphere calculations), we express our line acceleration parameter $\hat{g}_0$ in terms of $\hat{v}_\infty$ by means of Eq. (40), i.e.

$$\hat{g}_0 = \left(\frac{\hat{v}_\infty^2}{2} + \frac{\hat{v}_{\rm crit}^2}{\hat{r}_0^{1/\delta}}\right)\hat{r}_0\,\delta\,(1+\gamma), \tag{42}$$

and insert it into Eq. (39), as to obtain

$$\hat{v}\,(\hat{r}) = \sqrt{\frac{2}{\hat{r}_0}\left(\hat{v}_{\rm crit}^2\left(\frac{\hat{r}_0}{\hat{r}} - \hat{r}_0^{1-1/\delta}\right) + \left(\frac{\hat{r}_0}{2}\hat{v}_\infty^2 + \hat{v}_{\rm crit}^2\,\hat{r}_0^{1-1/\delta}\right)\left(1 - \frac{\hat{r}_0}{\hat{r}^\delta}\right)^{1+\gamma}\right)}, \tag{43}$$

which now depends on $\hat{v}_\infty$, $\gamma$, $\delta$ and $\hat{r}_0$.

Since $\delta$ is of the order of 1, as is $\hat{r}_0$, one can approximate the expression $\hat{r}_0^{1-1/\delta}$ in Eq. (43) as 1. Furthermore, as our line parameter $\hat{r}_0$ is defined as the parameter for which the line acceleration becomes zero at radius $\hat{r} = \hat{r}_0^{1/\delta}$ (cf. Eq. (14)), this radius is very close to the radius $\hat{r}_0'$ in the $\beta$-law (in Eq. (41)), where the wind velocity is assumed to be zero, i.e. $\hat{r}_0' \approx \hat{r}_0$.

Then, we can set the velocity in Eq. (41) equal to our velocity law in Eq. (43), to search for a relationship between the parameters $\beta$, $\gamma$ and $\delta$, which yields

$$\left(1 - \frac{\hat{r}_0}{\hat{r}}\right)^{2\beta-1} \overset{!}{\approx} -b + (1+b)\,\frac{\left(1 - \frac{\hat{r}_0}{\hat{r}^\delta}\right)^{1+\gamma}}{\left(1 - \frac{\hat{r}_0}{\hat{r}}\right)} \tag{44}$$

with

$$b := \frac{2}{\hat{r}_0}\left(\frac{\hat{v}_{\rm crit}}{\hat{v}_\infty}\right)^2.$$

Herein, for large radii $\hat{r}$ (and especially for small values of $b$, e.g. $b \lesssim 0.1$ for an O-V-star), the right hand side can be approximated by the last fraction only, which leads to

$$\left(1 - \frac{\hat{r}_0}{\hat{r}}\right)^{2\beta} \overset{!}{\approx} \left(1 - \frac{\hat{r}_0}{\hat{r}^\delta}\right)^{1+\gamma}, \tag{45}$$

or equivalently

$$\frac{2\beta}{1+\gamma} \approx \frac{\log\left(1 - \frac{\hat{r}_0}{\hat{r}^\delta}\right)}{\log\left(1 - \frac{\hat{r}_0}{\hat{r}}\right)}. \tag{46}$$

Next, the righthand side in Eq. (46) can be approximately set to 1, for values of $\delta \longrightarrow 1$ or generally for smaller distances from the central star in the supersonic region as $\hat{r} \longrightarrow \hat{r}_0^{1/\delta} \approx 1$. This results the desired relationship between $\beta$ and $\gamma$

$$2\beta \approx 1 + \gamma, \tag{47}$$

independent of $\delta$, that is most valid for the previously mentioned values for $\delta$ at smaller radii $\hat{r}$. It also applies at very large distances $\hat{r} \gg 1$, since then, the numerical values inside the brackets of Eq. (45) are close to 1 and this equation is fulfilled for any value of the exponents $\beta$ and $\gamma$ in all cases. Only for intermediate distances from the star at lower values of $\delta$ (not close to 1), the relationship between $\beta$ and $\gamma$ is possibly not well approximated by Eq. (47).

Figure 6 illustrates this described behaviour by the comparison of the approximated wind solution with the $\beta$ law for our wind model calculations from a typical O5-V-star.

#### 2.5.7. Fitting formula for the line acceleration

Thus, we can provide another expression for the line acceleration (in Eq. (14)), now dependent on $\hat{v}_\infty$ and on the parameters $\beta$ (or $\gamma$ respectively), $\delta$ and $\hat{r}_0$ (by eliminating $\hat{g}_0$ using Eq. (42)):

$$\hat{g}_{\rm rad}^{\rm line}(\hat{r}) = \left( \frac{\hat{v}_\infty^2}{2} + \frac{\hat{v}_{\rm crit}^2}{\hat{r}_0^{1/\delta}} \right) \hat{r}_0 \, \delta \, (1+\gamma) \, \frac{1}{\hat{r}^{1+\delta}} \left( 1 - \frac{\hat{r}_0}{\hat{r}^\delta} \right)^\gamma , \tag{48}$$

or

$$\hat{g}_{\rm rad}^{\rm line}(\hat{r}) = \left( \hat{v}_\infty^2 + \frac{2\,\hat{v}_{\rm crit}^2}{\hat{r}_0^{1/\delta}} \right) \hat{r}_0 \, \delta \, \beta \, \frac{1}{\hat{r}^{1+\delta}} \left( 1 - \frac{\hat{r}_0}{\hat{r}^\delta} \right)^{2\beta-1} . \tag{49}$$

Both of these non-linear expressions can then be used as fitting formulae and applied to the results from a numerical calculation of $\hat{g}_{\rm rad}^{\rm line}(\hat{r}_i)$ for discrete radial grid points $\hat{r}_i$, in order to determine the line acceleration parameters $\gamma$ (or equivalently $\beta$), $\delta$ and $\hat{r}_0$, and the terminal velocity $\hat{v}_\infty$ (cf. Fig. 1).

#### 2.5.8. Physical interpretation of the equation of critical radius

Through the use of the exact wind solution, by using Eq. (18), valid for the critical radius $\hat{r}_{\rm c}$, we can solve for the line acceleration parameter $\hat{g}_0$ and insert it into Eq. (40) from the approximated wind solution, to provide another expression for the terminal velocity depending on the location of the critical (i.e. sonic) point

$$\hat{v}_\infty = \sqrt{ \frac{2}{\hat{r}_0} \left( \left( \frac{\hat{r}_{\rm c}^\delta}{\hat{r}_{\rm c}^\delta - \hat{r}_0} \right)^\gamma \frac{\hat{r}_{\rm c}^{\delta-1}}{\delta\,(1+\gamma)} \left( \hat{v}_{\rm crit}^2 - 2\,\hat{r}_{\rm c} \right) - \hat{v}_{\rm crit}^2 \hat{r}_0^{1-1/\delta} \right) } . \tag{50}$$

Or vice versa, by Eq. (18), the location of the critical point (through which the exact analytical wind solution of our equation of motion EOM (16) passes) is mainly determined, on the one hand, by the given terminal velocity $v_\infty$, via the line acceleration parameter $\hat{g}_0$. On the other hand, the position of $\hat{r}_{\rm c}$ must also be dependent on the given minimum velocity $v_{\rm in}$ at the inner boundary radius $R_{\rm in}$, where the velocity solution passes. This inner velocity $v_{\rm in}$ follows indirectly from the other remaining line acceleration or wind parameters $\gamma$, $\delta$ (which make up the shape of the velocity curve) and especially $\hat{r}_0$ (where the value of the latter parameter is determined by the radius $\hat{r}_0^{1/\delta}$ at which $g_{\rm rad}^{\rm line}$ is zero).

Since the inner boundary condition of the velocity $v_{\rm in}$ is connected to the mass-loss rate $\dot{M}$, through the equation of mass continuity by Eq. (8) and the given density at the inner boundary, the position of the critical radius is uniquely specified by the values of $v_\infty$ and $\dot{M}$.

#### 2.5.9. The reasons for deriving the approximated solution

The reason for the derivation of our *approximated* wind solution (in Sect. 2.5.5), that is only valid in the supersonic approximation, is *not* its application to represent the unique wind solution in the whole wind regime (i.e. including the subsonic region). The approximated solution is required to be able to calculate the terminal velocity $v_\infty$ belonging to our exact analytical wind solution described by Eqs. (30) and (31) and to overcome its artificial and unlimited increase with increasing radius by assuming an isothermal wind (as discussed at the end of Sect. 2.5.4).

In other words: the approximated solution is necessary to be able (1) to find the relation between $v_\infty$ and the line acceleration (or wind) parameters $\hat{g}_0$, $\gamma$, $\delta$ and $\hat{r}_0$, and (2) to compare the exponents $\gamma$ and $\delta$ to the exponent $\beta$ (in the $\beta$-law).

This, in turn, is necessary because our applied model atmosphere code assumes a $\beta$-velocity law for the whole supersonic wind region which is mainly determined by the input parameters $v_\infty$ and $\beta$. The additionally used code parameter $\hat{r}_0'$ (cf. Eq. (41)) is related to the velocity $v_{\rm in}$ at the inner boundary radius which, again, is directely dependent on the prescribed mass-loss rate $\dot{M}$ via the continuity Eq. (8) (and the density at the inner boundary given therein).

## 3. Numerical methods

### 3.1. Computing the radiative acceleration

The calculation of the radiative acceleration of a stellar wind requires the numerical computation of the contribution of a very large number of spectral lines. We first calculate the thermal, density and ionisation structure of the wind model by means of the non-LTE expanding atmosphere (improved Sobolev approximation) code ISA-Wind (de Koter et al. 1993, 1997). As a next step, we calculate the radiative acceleration as a function of distance by means of a Monte Carlo (MC) code MC-Wind (de Koter et al. 1997; Vink et al. 1999). The basic ideas behind this technique were first applied to the study of stellar winds from early-type stars by Abbott & Lucy (1985), but in our calculation we account for the possibility that the photons can be scattered or absorbed and re-emitted (due to real absorption) or eliminated (if they are scattered back into the star).

The radiative transfer in MC-Wind involves multiple continuum and line processes using the Sobolev approximation. The continuum processes include electron scattering and thermal absorption and emission, whilst the line processes include photon scattering and photon destruction by collisional de-excitation. Line processes can only occur at specific points in each shell of the stellar wind, whereas continuum processes can occur at any point. To decide whether a continuum or line process takes place, we apply a similar approach to Mazzali & Lucy (1993), where a random optical depth value is compared to the combined optical depth for line and continuum processes along a photon's path. Our code was improved in the following way: after it is decided that the next process will be a continuum process, a second random number is generated to decide which continuum process takes place, an electron scattering or absorption process (as implemented in Vink et al. 1999; Vink 2000).

The radiative acceleration of the wind is calculated by following the fate of the large number of photons where the atmosphere is divided into a large number of concentric thin shells with radius $r$ and thickness d$r$, and the loss of photon energy, due to all scatterings that occur within each shell, is determined.

The total line acceleration per shell summed over all line scatterings in that shell equals (Abbott & Lucy 1985)

$$g_{\rm rad}^{\rm line}(r) = -\frac{1}{\dot{M}}\frac{{\rm d}L(r)}{{\rm d}r}, \tag{51}$$

where $-{\rm d}L(r)$ is the rate at which the radiation field loses energy by the transfer of momentum of the photons to the ions of the wind per time interval.

The line list that is used for the MC calculations consists of over $10^5$ of the strongest lines of the elements from H to Zn from a line list constructed by Kurucz (1988). Lines in the wavelength region between 50 and 10 000 Å are included with ionisation stages up to stage VII. The number of photon packets distributed over the spectrum in our wind model, followed from the lower boundary of the atmosphere, is $2 \times 10^7$. The wind is divided into 90 spherical shells with a large number of narrow shells in the subsonic region and wider shells in the supersonic range.

### 3.2. Computing the mass-loss rate for known stellar and wind parameters

By neglecting the pressure term and using the expression for the line acceleration per shell (Eq. (51)), an integration of the equation of motion (10), from stellar radius to infinity, yields (cf. Abbott & Lucy 1985)

$$\frac{1}{2}\dot{M}\left(v_\infty^2 + v_{\rm esc}^2\right) = \Delta L,$$

or equivalently,

$$\dot{M} = \frac{2\,\Delta L}{v_\infty^2 + v_{\rm esc}^2}, \tag{52}$$

where $\Delta L$ is the total amount of radiative energy extracted per second, summed over all the shells. This equation is now fundamental for determining mass-loss rates numerically from the total removed radiative luminosity, for the prespecified stellar and wind parameters $v_{\rm esc}$ and $v_\infty$, respectively.

### 3.3. The iteration method: determination of $\dot{M}$ and the wind parameters

In computing the mass-loss rate and the wind model parameters from a given central star with fixed stellar parameters $L$, $T_{\rm eff}$, $R$, $M$, $\Gamma$, the following iterative procedure is applied:

1. By keeping the stellar and wind parameters $\dot{M}_n$, $v_{\infty_n}$, $\beta_n$ variable throughout our iteration process, we use arbitrary (but reasonable) starting values $\dot{M}_{-1}$, $v_{\infty_{-1}}$, $\beta_{-1}$ in iteration step $n = -1$ (cf. Tables 2–4).
2. For these input parameters, a model atmosphere is calculated with ISA-Wind. The code yields the thermal structure, the ionisation and excitation structure, and the population of energy levels of all relevant ions. Then, the radiative acceleration $g_{\rm rad}^{\rm line}(r_i)$ is calculated for discrete radial grid points $r_i$ with MC-Wind and Eq. (51). In addition, an improved estimate for the mass-loss rate $\dot{M}_n^{\rm out}$ is obtained by Eq. (52), which can be used as a new input value for the next iteration step. Moreover, one obtains a new output value for the sonic radius $\hat{r}_{{\rm s}_n}$ (which has to be equal to the critical radius $\hat{r}_{\rm c}$ of our wind theory).
3. To determine the improved line acceleration parameters $\gamma_n$ (or equivalently $\beta_n$), $\delta_n$ and $\hat{r}_{0_n}$, Eq. (48) or (49) is used as the fitting formula to apply to the numerical results for $g_{\rm rad}^{\rm line}(r_i)$, cf. Fig. 1.
4. By applying Eq. (50) and inserting the current values of parameters $\gamma_n$, $\delta_n$ and $\hat{r}_{0_n}$, as well as the current sonic radius $\hat{r}_{{\rm s}_n}$ for $\hat{r}_{\rm c}$, we obtain a new approximation of the terminal velocity $v_{\infty_n}$, i.e.

$$\frac{v_{\infty_n}}{a} = \sqrt{\frac{2}{\hat{r}_{0_n}}\left(\left(\frac{\hat{r}_{{\rm s}_n}^{\delta_n}}{\hat{r}_{{\rm s}_n}^{\delta_n} - \hat{r}_{0_n}}\right)^{\gamma_n}\frac{\hat{r}_{{\rm s}_n}^{\delta_n - 1}}{\delta_n\,(1+\gamma_n)}\left(\hat{v}_{\rm crit}^2 - 2\,\hat{r}_{{\rm s}_n}\right) - \hat{v}_{\rm crit}^2\,\hat{r}_{0_n}^{1-1/\delta_n}\right)}. \tag{53}$$

5. With these improved estimates of $\dot{M}_n$, $v_{\infty_n}$, $\beta_n$ as new input parameters, the whole iteration step, defined by items 2–4, is repeated until convergence is achieved.

### 3.4. Physical explanation of the iteration method for calculating the unique wind solution

In ISA-Wind the equation of motion is not solved explicitly for the supersonic wind region and, additionally, under the assumption of any input values of the stellar and wind parameters $\dot{M}$, $v_\infty$ and $\beta$, any arbitrary "solution" for the wind velocity field is conceivable. However, as from the theoretical point of view, it must be $\hat{r}_{\rm c} \equiv \hat{r}_{\rm s}$. Hence, to find numerically the unique wind solution by application of ISA-Wind, Eq. (53) guarantees that *at the end* of the iteration process this condition $\hat{r}_{\rm c} \equiv \hat{r}_{\rm s}$ is just fulfilled for the sonic radius $\hat{r}_{\rm s}$ in ISA-Wind for the converged set of wind parameters.

Equation (53) follows from this condition for the critical radius inserted into Eq. (18). Since the line acceleration parameter $\hat{g}_0$ can be expressed by means of the remaining parameters ($\gamma$, $\delta$, $\hat{r}_0$) via the terminal velocity $v_\infty$ (cf. Sects. 2.5.8 and 2.5.9), Eq. (40) has additionally been engaged for its derivation.

Thus, Eq. (53) determines the terminal velocity $v_{\infty_n}$ that our exact wind solution of the EOM (16) would need to have, in order to pass through the critical point at radius $\hat{r}_{{\rm c}_n} = \hat{r}_{{\rm s}_n}$ for the parameters of the fit to the numerical line acceleration curve obtained previously in the same iteration step ($\gamma_n$, $\delta_n$, $\hat{r}_{0_n}$). This improved estimate of $v_{\infty_n}$ is then used as a new input parameter in ISA-Wind for the terminal velocity in the next iteration step.

Naturally, the (current) position of the critical point is also affected by the parameter value of $\dot{M}_n$, since the value of $\dot{M}$ is simultaneously being determined iteratively and numerically together with the other remaining wind parameters by MC-Wind and ISA-Wind (with its assumed velocity- and density field) in our iteration process. By the improved estimate of $\dot{M}$ at each iteration step and the use of ISA-Wind, the lower boundary wind velocity $v_{\rm in}$ (at the inner boundary radius) is also gradually being adapted to an improved value (via the continuity Eq. (8) and the given inner boundary density).

Finally, at the end of the iteration process in the case of the convergence of all wind parameters, both different wind velocity curves (i.e. the exact solution of EOM (16) and the wind curve computed by ISA-Wind) share the same sonic point, i.e. intersect each other at radius $\hat{r}_{\rm s}$ (see Fig. 8), in order to approach the same terminal velocity value $v_\infty$ at large distances from the central star as $\hat{r} \to \infty$ (cf. Fig. 6).

Then, our exact wind solution, analytically expressed by Eqs. (30) and (31), fulfills the EOM (16) for the converged wind parameters $\hat{g}_0$ (or $v_\infty$), $\gamma$, $\delta$, $\hat{r}_0$. It now represents the unique wind

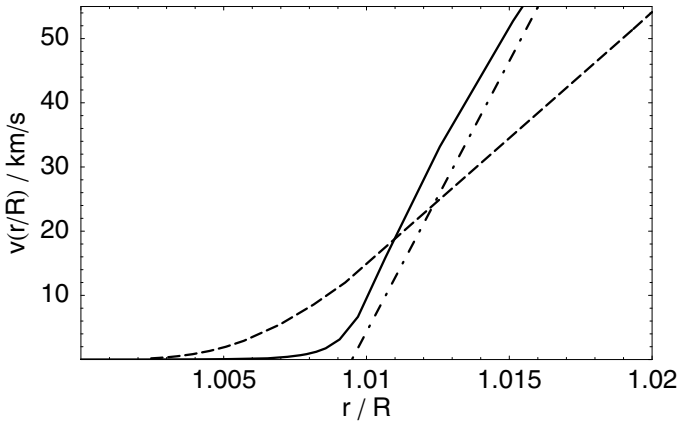


**Fig. 8.** The numerically computed wind velocity (assumed by ISA-WIND, see solid line) in comparison to the exact wind solution (dashed line) and the $\beta$ wind velocity curve (dotted-dashed line), also used in ISA-WIND, vs. radial distance $\hat{r}$ (in units of $R = 11.757\ R_\odot$) close to the O5-V central star (in Sect. 4). The *exact* solution fulfills the equation of motion (16) for the converged parameter values $\hat{g}_0 = 17661$, $\gamma = 0.4758$, $\delta = 0.6878$ and $\hat{r}_0 = 1.0016$ (shown in the last row of Table 2), at the end of the iteration process described in Sect. 3.3. In this case of convergence, the critical radius $\hat{r}_c$ of the equation of motion (16), determined by Eq. (18), becomes equal to the sonic radius $\hat{r}_s = 1.011$ determined by ISA-WIND (as demanded by our theory and iteration method). At this radius $\hat{r} = 1.011$, both wind velocity curves, i.e. the exact and the computed velocity curve by ISA-WIND, intersect each other.

solution through the critical point of the EOM (16) for the wind from a given star with fixed stellar parameters $L$, $T_{\rm eff}$, $R$, $M$, $\Gamma$.

### 3.5. The model assumptions and velocity field in the atmosphere code ISA-Wind

The ISA-WIND code has been described in detail by de Koter et al. (1993, 1996). Here, we will only discuss those model assumptions in ISA-WIND which affect our wind formalism by using the code in our iteration process.

In ISA-WIND the wind velocity structure is divided into two regions:

1. the low-velocity subsonic region determined by an EOM, similar to our Eq. (16), *however* in contrast to this, neglecting the line acceleration term, and, with an additional term $\propto {\rm d}T/{\rm d}r$ on the rhs of the equation (assuming a non-isothermal wind); and
2. the high-velocity supersonic region where the $\beta$ velocity law in Eq. (41) is assumed to represent the wind solution of the EOM (i.e. including then the line radiation forces).

These two regions are connected at a radius $\hat{r}_{\rm con}$, which is determined, together with the parameter $\hat{r}'_0$ (in Eq. (41)), with the condition that the velocity law is continuous in $v$ and ${\rm d}v/{\rm d}r$ at this connection radius. The value of $\hat{r}_{\rm con}$ is generally located close to and below the sonic point $\hat{r}_s$ (cf., e.g., Fig. 8, where $\hat{r}_{\rm con} = 1.010$, $\hat{r}'_0 = 1.0095$ and $\hat{r}_s = 1.011$).

The inner boundary condition of the flow velocity, $v_{\rm in}$ at the inner boundary radius $R_{\rm in}$, follows from prescribed (i.e. freely selectable) values of the density at the inner boundary condition and mass-loss rate (through the equation of mass continuity in form of Eq. (8)). Typically $R_{\rm in}$ is chosen to be situated at a Rosseland optical depth of $\tau_{\rm R} \gtrsim 20$. Therefore, $R_{\rm in}$ does *not* correspond to the stellar (i.e. phostospheric) radius $R$, that depends significantly on frequency. In ISA-WIND the photospheric radius $R_{\rm phot}$ is defined as the point where the thermal optical depth at 5555 Å equals $\tau_{\rm e} = 1/\sqrt{3}$. In practice is $R_{\rm in} < R_{\rm phot}$.

Hence, $R_{\rm phot}$ follows from the model computation and the chosen model parameters describing the density and velocity structure in the photosphere: the radius $R_{\rm in}$ and density $\rho_{\rm in}$ at the inner boundary. The wind is specified by the input parameters $\dot{M}$, $v_\infty$ and $\beta$. The parameters specifying the temperature structure are the luminosity $L$, $R_{\rm in}$ and the minimum temperature $T_{\rm min}$ (the value below which the wind temperature is not allowed to drop).

**Table 1.** The different starting values in the iterations A−C for the wind from an O5-V main-sequence star[a].

| Iteration | $v_\infty$ [km s$^{-1}$] | log $\dot{M}$ [$M_\odot$/ yr] |
|---|---|---|
| A | 2020.0 | –5.5 |
| B | 6000.0 | –7.0 |
| C | 2020.0 | –7.0 |

[a] For the stellar parameters, see Sect. 4.

### 3.6. The adjustment of the wind formalism to ISA-Wind

To be able to apply the analytical wind solution of our EOM (16) to model a stellar wind from a given central star (with fixed stellar parameters) by using ISA-WIND to find numerically the unique solution, we had to adjust our wind formalism, i.e. our more accurate EOM, to the assumed EOM and wind velocity structure in ISA-WIND. The EOM (16) (and therefore our exact analytical wind solution) considers (allows) a line acceleration throughout the whole wind regime, starting above the radius $\hat{r}_0^{1/\delta}$, whereas the different EOM in ISA-WIND is only solved in the subsonic region by neglecting the line force. However then, ISA-WIND "switches on" the line force somewhere below the connection radius $\hat{r}_{\rm con}$ in the subsonic region by assuming a $\beta$ velocity law above $\hat{r}_{\rm con}$ in the supersonic region.

This inconsistency through the use of ISA-WIND (compared to our model assumptions and solutions) has been eliminated by introducing the parameter $\hat{r}_0$ into our formalism for which the line radiation force is zero at radius $\hat{r}_0^{1/\delta}$. Then, the final value of $\hat{r}_0$, together with the other remaining line acceleration or wind parameters, can be determined by fitting Eq. (48) and the iteration procedure.

Further, since ISA-WIND begins its computations already *below* (however close to) the stellar (i.e. photospheric) radius, all formulae derived in Sect. 2 have thus been applied with reference to the inner boundary (core) radius $R_{\rm in}$ from where the numerical calculations of the wind model start. Therefore, the dimensionless variable of distance $\hat{r}$ here refers to $R = R_{\rm in}$ (see the wind model for a typical O main-sequence star in Sect. 4 and the associated diagrams in Sect. 2).

### 3.7. The chosen boundary values in the wind model

In our following numerical wind model the inner boundary radius has been chosen (constant throughout the whole iteration process) to be $R_{\rm in} = 11.757\ R_\odot$, situated at a fixed Rosseland optical depth of $\tau_{\rm R} = 23$. This corresponds then to a photospheric (stellar) radius of $R_{\rm phot} = 11.828\ R_\odot$ (defined as where the

**Table 2.** Iteration A for the wind from an O5-V main-sequence star. The variable stellar and wind parameters at each iteration step until convergence[a].

| Step No. | $v_\infty$ [km s$^{-1}$] | log $\dot{M}$ [$M_\odot$/ yr] | $v_{\infty,\mathrm{fit}}$ [km s$^{-1}$] | $\beta$ | $\gamma_{\mathrm{fit}}$ | $\delta_{\mathrm{fit}}$ | $\hat{r}_{0,\mathrm{fit}}$ | $\hat{r}'_0$ | $\hat{r}_\mathrm{s}$ |
|---|---|---|---|---|---|---|---|---|---|
| –1 | 2020 | –5.500 | – | 1.0000 | – | – | – | – | – |
| 0 | 6403 | –5.641 | 2365 | 0.8664 | 0.7329 | 0.4917 | 1.0008 | 1.0066 | 1.0175 |
| 1 | 4022 | –6.194 | 3846 | 0.7981 | 0.5963 | 0.7048 | 0.9999 | 1.0087 | 1.0101 |
| 2 | 3146 | –6.278 | 4106 | 0.7598 | 0.5195 | 0.8036 | 1.0020 | 1.0099 | 1.0113 |
| 3 | 3003 | –6.226 | 3909 | 0.7355 | 0.4711 | 0.7747 | 1.0030 | 1.0101 | 1.0115 |
| 4 | 2870 | –6.181 | 3760 | 0.7186 | 0.4372 | 0.7381 | 1.0027 | 1.0100 | 1.0113 |
| 5 | 2827 | –6.141 | 3684 | 0.7047 | 0.4094 | 0.6882 | 1.0024 | 1.0100 | 1.0111 |
| 6 | 2603 | –6.119 | 3495 | 0.7112 | 0.4224 | 0.7203 | 1.0003 | 1.0100 | 1.0110 |
| 7 | 2450 | –6.078 | 3301 | 0.7352 | 0.4704 | 0.7349 | 0.9940 | 1.0099 | 1.0111 |
| 8 | 2652 | –6.038 | 3124 | 0.7538 | 0.5075 | 0.7290 | 0.9939 | 1.0096 | 1.0112 |
| 9 | 3211 | –6.047 | 3232 | 0.7379 | 0.4758 | 0.6878 | 1.0016 | 1.0095 | 1.0112 |

[a] For the fixed stellar parameters $L$, $T_{\mathrm{eff}}$, $R$, $M$, and $\Gamma$, see Sect. 4. The line acceleration parameters $\gamma_{\mathrm{fit}}$ (or equivalently $\beta$), $\delta_{\mathrm{fit}}$ and $\hat{r}_{0,\mathrm{fit}}$, and the terminal velocity $v_{\infty,\mathrm{fit}}$, were determined by the fitting formula Eq. (48) (or Eq. (49)), applied to the results from a numerical calculation of the line acceleration $\hat{g}^{\mathrm{line}}_{\mathrm{rad}}(\hat{r}_i)$. The parameter $\hat{r}'_0$ (in the $\beta$ velocity law, Eq. (41)) and the sonic radius $\hat{r}_\mathrm{s}$ are output values from ISA-Wind, whereas log $\dot{M}$ is the improved estimated mass-loss rate numerically obtained (by MC-Wind and Eq. (52)). At each iteration step, the value of $v_\infty$ was calculated by Eq. (53) and used as the new input value for the terminal velocity in the next iteration step, together with the new estimates of $\dot{M}$ and $\beta$ (cf. description of iteration process in Sect. 3.3). Convergence is achieved when the values of $v_{\infty,\mathrm{fit}}$ and $v_\infty$ have become equal (i.e. here, close) to each other. In this case, the condition that the critical radius $\hat{r}_\mathrm{c}$ (determined by Eq. (18)) has to be equal to the sonic radius $\hat{r}_\mathrm{s} = 1.011$ (determined by ISA-Wind) is fulfilled.

**Table 3.** Iteration B for the wind from an O5-V main-sequence star. The variable stellar and wind parameters at each iteration step until convergence[a].

| Step No. | $v_\infty$ [km s$^{-1}$] | log $\dot{M}$ [$M_\odot$/ yr] | $v_{\infty,\mathrm{fit}}$ [km s$^{-1}$] | $\beta$ | $\gamma_{\mathrm{fit}}$ | $\delta_{\mathrm{fit}}$ | $\hat{r}_{0,\mathrm{fit}}$ | $\hat{r}'_0$ | $\hat{r}_\mathrm{s}$ |
|---|---|---|---|---|---|---|---|---|---|
| –1 | 6000 | –7.000 | – | 1.0000 | – | – | – | – | – |
| 0 | 4208 | –6.863 | 7011 | 1.0058 | 1.0116 | 1.3468 | 0.9976 | 1.0107 | 1.0142 |
| 1 | 4396 | –6.655 | 5511 | 0.9347 | 0.8695 | 1.1506 | 1.0042 | 1.0100 | 1.0153 |
| 2 | 3683 | –6.561 | 4968 | 0.9020 | 0.8040 | 1.1385 | 1.0002 | 1.0101 | 1.0135 |
| 3 | 3861 | –6.436 | 4588 | 0.8275 | 0.6550 | 0.9511 | 1.0051 | 1.0099 | 1.0133 |
| 4 | 3291 | –6.385 | 4432 | 0.7843 | 0.5687 | 0.9136 | 1.0039 | 1.0102 | 1.0121 |
| 5 | 3116 | –6.297 | 4152 | 0.7535 | 0.5070 | 0.8314 | 1.0036 | 1.0102 | 1.0118 |
| 6 | 2849 | –6.230 | 3922 | 0.7416 | 0.4833 | 0.7919 | 1.0014 | 1.0101 | 1.0115 |
| 7 | 2716 | –6.165 | 3596 | 0.7422 | 0.4844 | 0.7875 | 0.9996 | 1.0100 | 1.0114 |
| 8 | 3311 | –6.117 | 3544 | 0.7118 | 0.4237 | 0.6827 | 1.0046 | 1.0098 | 1.0113 |
| 9 | 2768 | –6.163 | 3765 | 0.6948 | 0.3897 | 0.6935 | 1.0031 | 1.0100 | 1.0109 |
| 10 | 2321 | –6.120 | 3460 | 0.7213 | 0.4426 | 0.7561 | 0.9953 | 1.0101 | 1.0110 |
| 11 | 2922 | –6.041 | 3228 | 0.7198 | 0.4396 | 0.6698 | 1.0008 | 1.0097 | 1.0112 |
| 12 | 2629 | –6.080 | 3385 | 0.7286 | 0.4572 | 0.7009 | 0.9968 | 1.0097 | 1.0108 |
| 13 | 3022 | –6.063 | 3358 | 0.7168 | 0.4336 | 0.6633 | 1.0018 | 1.0097 | 1.0111 |
| 14 | 2493 | –6.102 | 3397 | 0.7334 | 0.4669 | 0.7447 | 0.9955 | 1.0098 | 1.0108 |
| 15 | 3008 | –6.056 | 3307 | 0.7225 | 0.4449 | 0.6696 | 1.0013 | 1.0097 | 1.0112 |

[a] See description of parameters, analogous to iteration A, in Table 2 above.

thermal optical depth is $\tau_\mathrm{e} = 1/\sqrt{3}$) and an inner boundary density of $\rho_{\mathrm{in}} = 1.398 \times 10^{-8}$ g/cm$^3$ at $R_{\mathrm{in}}$.

This particular chosen fixed value of $\tau_\mathrm{R}$ (or corresponding $\rho_{\mathrm{in}}$) at each step of the iteration cycle has no effect on the final wind parameters, i.e. in particular on the converged values of $\dot{M}$ and $v_\infty$, as further additional test iterations for a lower boundary value of $\tau_\mathrm{R} < 23$ (at the same $R_{\mathrm{in}}$) have shown. The reason why the exact value of $\rho_{\mathrm{in}}$ is irrelevant, is, because we ensure by our iteration scheme that the sonic point, determined by the ISA-Wind computations, is at each iteration step $n$ always located at the right radius, namely at the present critical radius of our EOM (16) and exact analytical solution. This current critical radius is valid for all the present estimates of updated wind parameter values obtained from the $g^{\mathrm{line}}_{\mathrm{rad}}$ curve fitting, i.e. in particular for $\dot{M}_n$ and $v_{\infty_n}$ (see further explanations in Sects. 2.5.8 and 3.4).

### 3.8. General aspects of the boundary conditions for the uniqueness of the solutions

To be able to solve the system of equations involving both the equation of continuity (7) and the momentum Eq. (10) uniquely, one boundary condition in each case is required. To solve the momentum equation for the velocity $v(r)$, the density variable $\rho$ was first eliminated by means of the equation of mass conservation, to obtain the density independent equation of motion. This

**Table 4.** Iteration C for the wind from an O5-V main-sequence star: the variable stellar and wind parameters at each iteration step until convergence[a].

| Step No. | $v_\infty$ [km s$^{-1}$] | log $\dot{M}$ [$M_\odot$/ yr] | $v_{\infty,\mathrm{fit}}$ [km s$^{-1}$] | $\beta$ | $\gamma_{\mathrm{fit}}$ | $\delta_{\mathrm{fit}}$ | $\hat{r}_{0,\mathrm{fit}}$ | $\hat{r}'_0$ | $\hat{r}_\mathrm{s}$ |
|---|---|---|---|---|---|---|---|---|---|
| –1 | 2020 | –7.000 | – | 1.0000 | – | – | – | – | – |
| 0 | 4161 | –6.448 | 4467 | 0.9230 | 0.8459 | 1.0278 | 1.0052 | 1.0097 | 1.0203 |
| 1 | 4080 | –6.430 | 4506 | 0.8463 | 0.6927 | 0.9593 | 1.0043 | 1.0097 | 1.0130 |
| 2 | 3431 | –6.407 | 4515 | 0.7937 | 0.5875 | 0.9191 | 1.0040 | 1.0101 | 1.0121 |
| 3 | 3340 | –6.326 | 4260 | 0.7553 | 0.5107 | 0.8416 | 1.0052 | 1.0102 | 1.0119 |
| 4 | 2791 | –6.272 | 4087 | 0.7300 | 0.4600 | 0.7965 | 1.0025 | 1.0102 | 1.0115 |
| 5 | 2619 | –6.179 | 3683 | 0.7321 | 0.4642 | 0.7760 | 0.9995 | 1.0101 | 1.0114 |
| 6 | 2924 | –6.111 | 3484 | 0.7251 | 0.4501 | 0.7078 | 1.0015 | 1.0099 | 1.0113 |
| 7 | 2917 | –6.116 | 3509 | 0.7098 | 0.4196 | 0.6994 | 1.0028 | 1.0098 | 1.0110 |
| 8 | 2752 | –6.116 | 3560 | 0.7073 | 0.4146 | 0.6899 | 1.0014 | 1.0099 | 1.0110 |
| 9 | 2688 | –6.094 | 3450 | 0.7084 | 0.4169 | 0.6930 | 1.0007 | 1.0099 | 1.0110 |
| 10 | 2800 | –6.076 | 3375 | 0.7052 | 0.4105 | 0.6833 | 1.0019 | 1.0098 | 1.0110 |
| 11 | 2828 | –6.082 | 3438 | 0.6978 | 0.3956 | 0.6657 | 1.0024 | 1.0098 | 1.0109 |
| 12 | 2416 | –6.090 | 3369 | 0.7119 | 0.4238 | 0.7133 | 0.9969 | 1.0099 | 1.0108 |
| 13 | 2572 | –6.039 | 3142 | 0.7394 | 0.4788 | 0.7235 | 0.9950 | 1.0097 | 1.0111 |
| 14 | 3087 | –6.035 | 3181 | 0.7320 | 0.4639 | 0.6859 | 1.0012 | 1.0095 | 1.0111 |

[a] See description of parameters, analogous to iteration A, in Table 2 above.

**Table 5.** The results of the different iterations A–C for the wind from an O5-V main-sequence star. The converged values of the wind parameters $v_\infty$, $\beta$, $\gamma$, $\delta$, $\hat{r}_0$ in the radiative line acceleration Eq. (48) (or Eq. (49), respectively), and mass-loss rate log $\dot{M}$ of each iteration cycle[a].

| Iteration | log $\dot{M}$ [$M_\odot$/ yr] | $v_\infty$ [km s$^{-1}$] | $\beta$ | $\gamma$ | $\delta$ | $\hat{r}_0$ | $\hat{r}_\mathrm{c}$ |
|---|---|---|---|---|---|---|---|
| A | –6.047 | 3232 | 0.7379 | 0.4758 | 0.6878 | 1.0016 | 1.0110 |
| B | –6.056 | 3307 | 0.7225 | 0.4449 | 0.6696 | 1.0013 | 1.0083 |
| C | –6.035 | 3181 | 0.7320 | 0.4639 | 0.6859 | 1.0012 | 1.0101 |
| Mean values | –6.046 ± 0.006 | 3240 ± 37 | 0.731 ± 0.005 | 0.462 ± 0.009 | 0.6811 ± 0.0001 | 1.0014 ± 0.0001 | 1.0098 |

[a] In addition, the critical radius $\hat{r}_\mathrm{c}$ (equal to the sonic radius $\hat{r}_\mathrm{s}$), determined by Eq. (18), is displayed in the last column, as it is needed as a further parameter to evaluate the wind solution by Eqs. (30) and (31). The mean parameter values (with error estimations) have been calculated from the results of all iterations A–C.

equation could then be solved uniquely for (e.g.) the wind velocity, because we demand a continuous and smooth trans-sonic flow through the critical point $\hat{r}_\mathrm{c}$ of Eq. (16) for a stellar wind as one boundary condition. However, to be able to also solve the equation of continuity (7) uniquely for the mass-loss rate $\dot{M}$ by integration, as in Eq. (8), knowledge of the density $\rho(r)$ for at least one local point $r$ is required as another physical constraint. Thus, the density stratification for a given stellar wind (and therefore $\dot{M}$) cannot be determined by merely using Eq. (8) with the $v(r)$ solution of the equation of motion.

In more general terms, it can be shown that all solutions ($v_\infty$, $\dot{M}$) lie on a curve, which fulfills the equation

$$\dot{M}\, v_\infty^q = \text{const.}, \quad \text{with} \quad q \approx 2, \tag{54}$$

since $1/2\, \dot{M}\, v_\infty^2$ corresponds to the total wind energy (per time interval, i.e. equal to the kinetic wind energy far away from the potential of the central star). Hence, by providing an additional boundary condition, as, e.g., a given observed value for $v_\infty$, the mass-loss rate would then be uniquely determined by a point on this curve (for which $\dot{M} = \text{const.}\, v_\infty^{-q}$).

However, since we are interested in self-consistent solutions, i.e. theoretical predictions of $v(r)$ *and* $\dot{M}$ for a certain wind model from a given central star, without any prior knowledge of the terminal velocity $v_\infty$, we follow the additional constraint that $R$ (i.e. the inner boundary radius $R_\mathrm{in}$) is situated at a fixed chosen optical depth $\tau(R)$, or corresponding fixed density $\rho(R)$ (cf. Sect. 3.7). The latter value is given by Eq. (9) and the values for $\dot{M}$ and $v(R)$, i.e. $v_\mathrm{in}$.

In our iteration process and by the use of ISA-Wind this criterion is always fulfilled at each iteration step. It is used to update (adapt) the value of $v(R)$ at the inner boundary radius of the velocity assumed in ISA-Wind, by means of the new estimate of $\dot{M}$ obtained by MC-Wind (and Eq. (52) that depends on the value of $v_\infty$). After all wind parameters have converged, the final position of the sonic radius $\hat{r}_\mathrm{s}$, i.e. the critical radius $\hat{r}_\mathrm{c}$ belonging to the point through which the unique final wind solution goes, is known.

Hence, to summarise the mathematical point of view, the second necessary boundary condition we have used to be able to solve our system of equations (consisting of Eqs. (7) and (10)), or in other words, to find the unique values of $\dot{M}$ and $v_\infty$, is to prescribe the location of the critical point to be at the *right* position, i.e. at the radius $\hat{r}_\mathrm{s}$ of the sonic point, while the density $\rho(R)$ at the inner boundary radius is kept at a fixed value.

## 4. Application: results for an O-star

In this section, we apply our theoretical results of Sect. 2 and the iterative procedure described in Sect. 3.3 to compute the stellar wind parameters for a typical O5-V main-sequence star. The

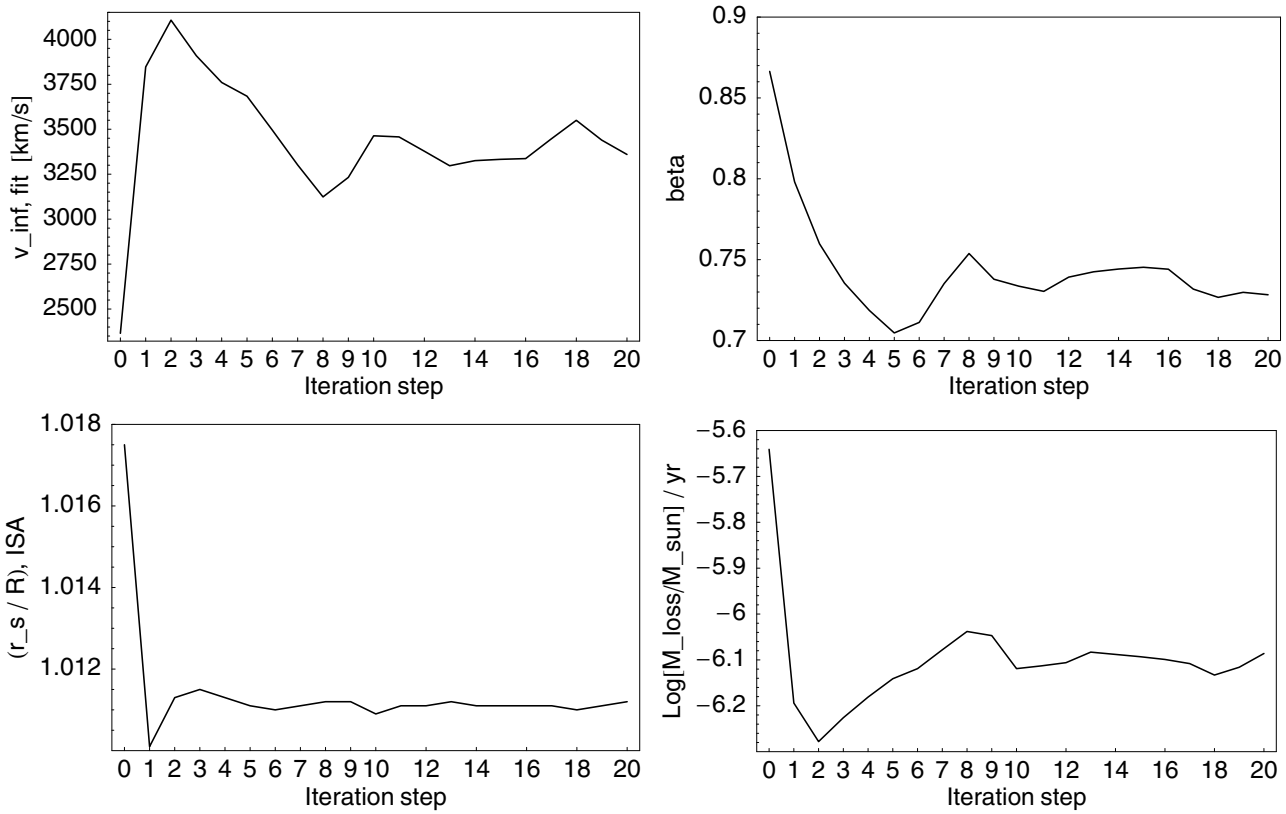


**Fig. 9.** Iteration A for the wind from an O5-V main-sequence star: the varying wind parameters $v_{\infty,\mathrm{fit}}$ (see *upper left* diagram) and $\beta$ (*upper right*), both obtained by the fitting to numerical results for the line acceleration, the numerically determined sonic radius $\hat{r}_\mathrm{s}$ (by ISA-WIND, see *lower left*), and the stellar mass-loss rate $\log \dot{M}$ (calculated by MC-Wind, see *lower right*), plotted versus the step numbers of iteration A until convergence. For the fixed stellar parameters $L$, $T_\mathrm{eff}$, $R$, $M$ and $\Gamma$, see Sect. 4. See also the description of parameters in Table 2.

fixed stellar parameters (see e.g. Martins et al. 2005, and references therein) are:

- $T_\mathrm{eff} = 40\,000$ K;
- $\Gamma = 0.214$;
- $R_\mathrm{core} = 11.757\,R_\odot$;
- $M = 40.0\,M_\odot$;
- $\log\,(L/L_\odot) = 5.5$;
- solar metallicity.

From which an isothermal sound speed of 18.16 $\mathrm{km\,s^{-1}}$ is obtained.

The iteration method is tested for convergence by three different iteration cycles A−C with three different starting values for $v_\infty$ and $\dot{M}$, see Table 1. The reason for choosing these particular values is to start the iteration process for $v_\infty$ and $\dot{M}$ values that are either significantly higher, or lower, or lower for both, than the expected values.

The results of each iteration step for each of the three iteration cycles are listed in Tables 2 to 4. In addition, some of these results are graphically displayed in Figs. 9 to 11, where the values of $v_\infty$, $\beta$, $\hat{r}_\mathrm{s}$, and $\log \dot{M}$, are plotted against the associated iteration step.

From this, we can state that for each of the three runs all stellar and wind parameters converge to the same values (within statistical fluctuations) within approximately 10 iteration steps. However, to achieve a higher precision it is partly necessary to perform up to 15 steps in one iteration (see Tables 3 and 4 of iteration B and C).

At the end of each iteration process A−C, we obtain the same converged radiative line acceleration $\hat{g}_\mathrm{rad}^\mathrm{line}\,(\hat{r})$ (see def. Eq. (12)) of our stellar wind model as, e.g., in case of iteration A, plotted versus radial distance $\hat{r}$ in Fig. 1. The dots represent the results from the numerical calculation of $\hat{g}_\mathrm{rad}^\mathrm{line}\,(\hat{r}_i)$ for discrete radial grid points $\hat{r}_i$. These numerical values are fitted well to the line acceleration function in Eq. (14) by the displayed fitting curve (solid line) with the (fitting, i.e. line) parameters $\hat{g}_0 = 17\,661$, $\gamma = 0.4758 \pm 0.0002$, $\delta = 0.6878 \pm 0.0003$ and $\hat{r}_0 = 1.0016$ (according to $v_\infty = 3232$ $\mathrm{km\,s^{-1}}$) at the end of iteration cycle A.to find the unique numerical solution The remaining converged stellar wind parameters (obtained by the same iteration cycle) as well as the resulting parameters from both other iterations B and C are listed in Table 5.

Convergence is achieved when both values of the terminal velocity $v_{\infty,\mathrm{fit}}$ and $v_\infty$, one obtained by the fitting formula Eq. (48) and the other by Eq. (53), have approached each other arbitrarily close (up to a desired precision). This is the case when the critical radius $\hat{r}_\mathrm{c}$ (determined by Eq. (18)) has become equal to the sonic radius $\hat{r}_\mathrm{s}$ (determined by ISA-WIND).

Finally, we can summarise the numerical results of all iterations A−C by the mean values in Table 5: $\log \dot{M} = -6.046 \pm 0.006\ M_\odot/\mathrm{yr}$, $v_\infty = 3240 \pm 37$ $\mathrm{km\,s^{-1}}$, $\beta = 0.731 \pm 0.005$, or $\gamma = 0.462 \pm 0.009$, $\delta = 0.6811 \pm 0.0001$ and $\hat{r}_0 = 1.0014 \pm 0.0001$ with an average critical (i.e. sonic) radius of $\hat{r}_\mathrm{c} = 1.0098$.

The model results for the wind velocity $\hat{v}\,(\hat{r})$ as a function of radial distance $\hat{r}$ from the typical O5-V-star, with the above mentioned converged wind and line acceleration parameters of iteration A, are displayed in Figs. 5−7 and have been already discussed in Sect. 2.5.

Figure 5 shows the comparison of the approximated and the exact wind solution with the converged line acceleration

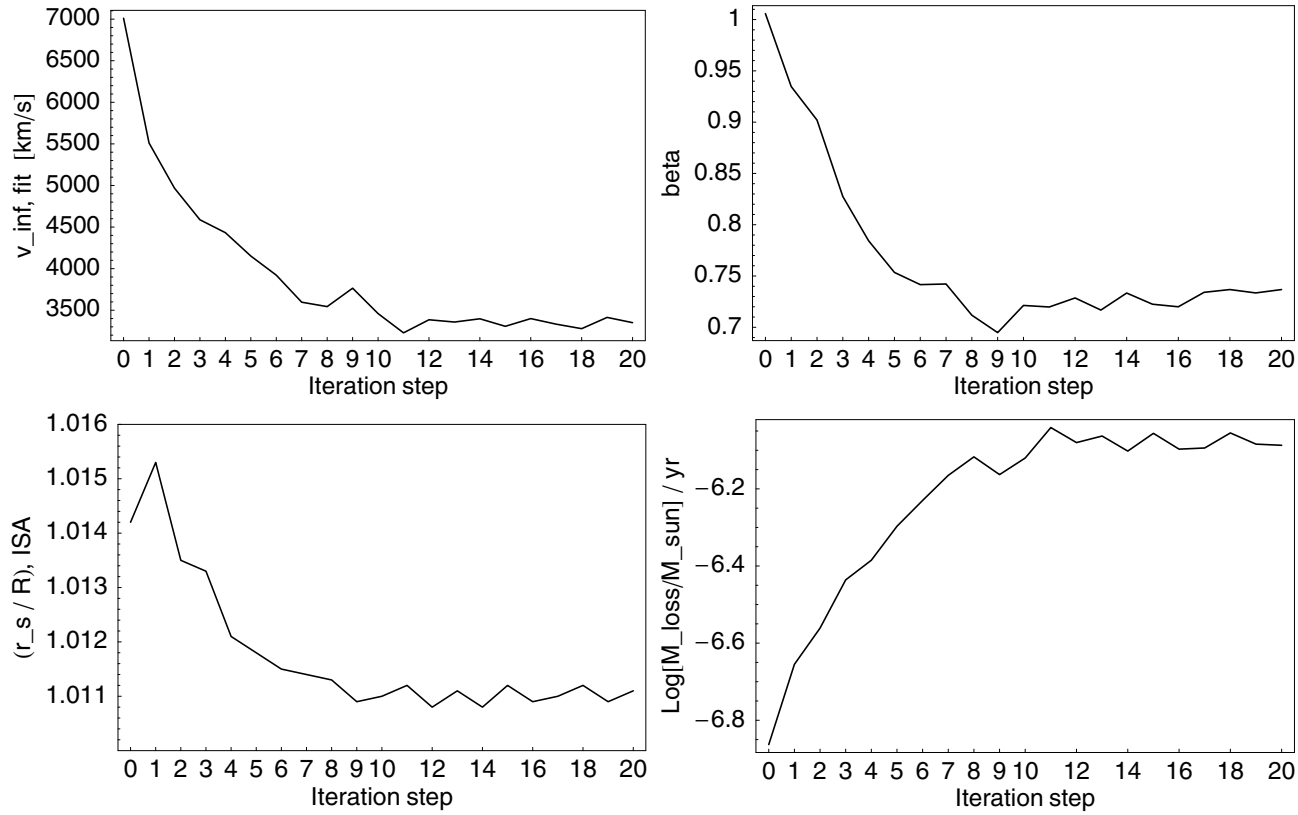


**Fig. 10.** Iteration B for the wind from an O5-V main-sequence star: the varying stellar and wind parameters $v_{\infty,\mathrm{fit}}$ (see *upper left* diagram), $\beta$ (*upper right*), both obtained by the fitting to numerical results for the line acceleration, the sonic radius $\hat{r}_\mathrm{s}$ (determined by ISA-WIND, see *lower left*), and the mass-loss rate $\log \dot{M}$ (calculated by MC-Wind, see *lower right*), plotted versus the step numbers of iteration B until convergence.

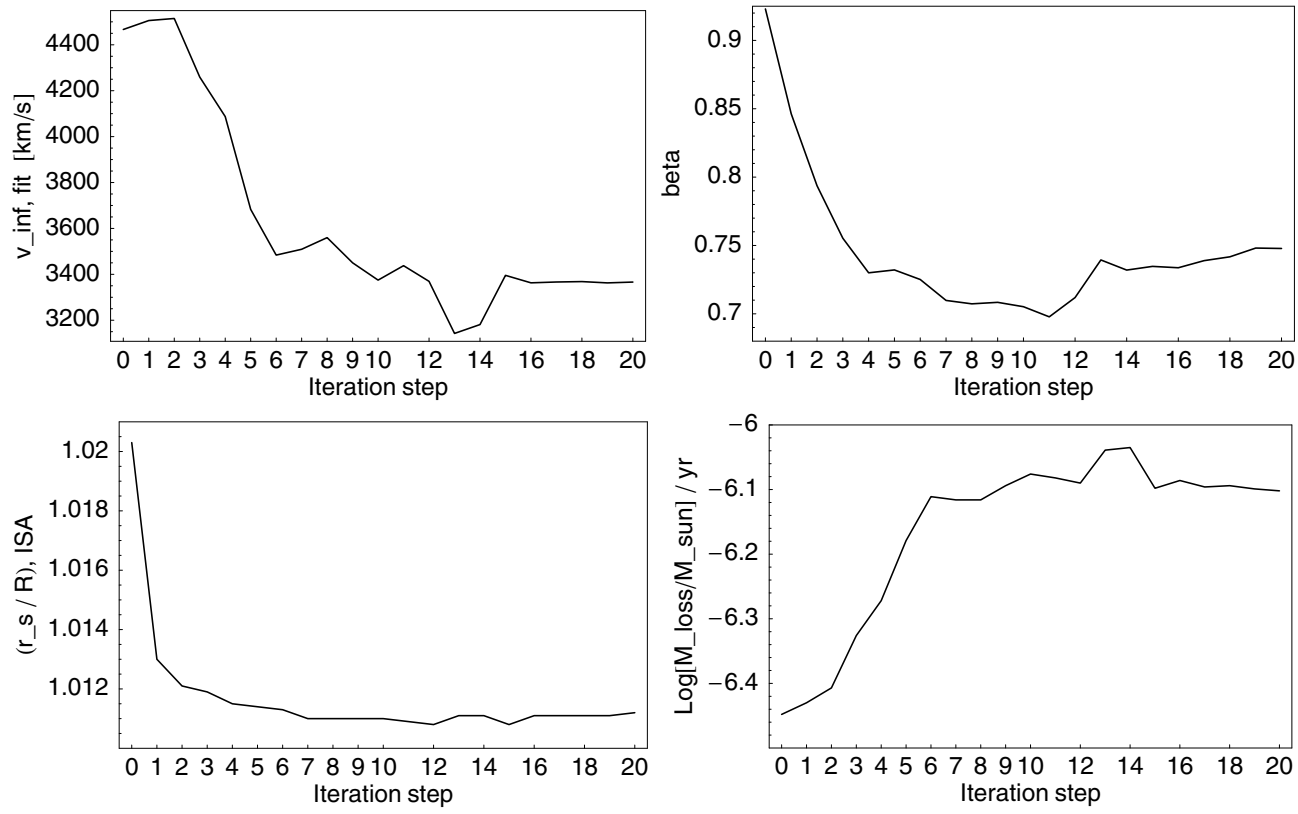


**Fig. 11.** Iteration C for the wind from an O5-V main-sequence star: the varying stellar and wind parameters $v_{\infty,\mathrm{fit}}$ (see *upper left* diagram), $\beta$ (*upper right*), both obtained by the fitting to numerical results for the line acceleration, the sonic radius $\hat{r}_\mathrm{s}$ (determined by ISA-WIND, see *lower left*), and the mass-loss rate $\log \dot{M}$ (calculated by MC-Wind, see *lower right*), plotted versus the step numbers of iteration C until convergence.

parameters $\hat{g}_0$, $\gamma$, $\delta$ and $\hat{r}_0$ of iteration A in Eq. (14), where the approximated wind curve was obtained using Eq. (39), whereas the exact wind solution was obtained from Eqs. (30), (31), and (33), with a critical radius of $\hat{r}_c = \hat{r}_s = 1.0110$. A more detailed comparison of the approximated and the exact wind solution is shown in Fig. 7, where both curves are displayed for three different radial ranges. The only noticeable discrepancy between the wind velocity curves is in the subsonic and sonic region where the approximated wind solution, derived for (and only supposed to be applied in) the supersonic region, is no longer valid. Figure 6 displays the same approximated wind solution together with the $\beta$ wind velocity curve, where the latter was obtained from Eq. (41) with the converged values for the exponent $\beta = 0.7379$ and the terminal velocity $v_\infty = 3232\ \mathrm{km\,s^{-1}}$ of iteration A (with $\hat{r}'_0 = 1.0095$ as used in ISA-Wind). Both curves approach each other and the same velocity limit $v_\infty$ at large radial distances $\hat{r}$.

These comparisons highlight the good agreement between all velocity curves in the supersonic region, except for the noticeable difference of the $\beta$- and approximated wind velocity curve at intermediate distances $\hat{r} \gtrsim 5$ from the star (see Fig. 6). In the supersonic region, the $\beta$ velocity curve always lies (e.g. at radial distance of $\hat{r} = 10$ by 12%, and at $\hat{r} = 100$ only by 3%) above the approximated solution. Compared to the exact wind solution, this means that the $\beta$-wind law overestimates the real wind velocity over the entire range of radial distances.

This difference at intermediate distances is mainly due to our approximation (Eq. (47)) for the relationship between the exponents $\beta$ and $\gamma$ (cf. the comparison of the $\beta$ law with our approximated velocity) that is only approximately independent of the exponent $\delta$, if the latter is close to 1. Since in our wind model the value of $\delta$ has actually converged to 0.7, this approximated relation does not provide a better value for $\beta$ to adapt the $\beta$ curve closer to the approximated (and also real) velocity curve in the middle wind regime. Nevertheless, we first had to introduce the additional exponent $\delta$ in our line acceleration function, Eq. (14), to gain an optimal fitting to the numerical calculation of $\hat{g}^{\mathrm{line}}_{\mathrm{rad}}(\hat{r})$ at those middle radial ranges of the wind.

## 5. Discussion and conclusions

In this paper, we have derived analytical solutions for the velocity structure for any mass outflow or inflow situation, through use of the Lambert $W$-function. For the case of a radiation-driven wind, we described the line acceleration as a function of stellar radius $g(r)$, and therefore found, as a mathematical consequence, the critical point of our equation of motion to be the sonic point (in contrast to the critical point of the different EOM of CAK).

The reason why the line acceleration can be expressed as a function of radius only can be justified as follows: by solving the basic hydrodynamic equations under the assumption of a stationary (i.e. steady) spherical flow, we assume that the problem is solvable time-independently and all physical quantities, in particular the solution functions, and especially the line acceleration must be expressable as a function of radius only. This occurs at the latest after the physical process has reached an equilibrium. The evidence is given by this work, where, at the end of three different iteration cycles, $g(r)$ converges to the same function of $r$ for the same stellar wind model.

The numerical calculation of $g(r)$ was performed through Monte Carlo simulations and the wind parameters were simultaneously solved in an iterative way for a typical O5-V star. Our computations converged to $\log \dot{M} = -6.05\ M_\odot/\mathrm{yr}$, $v_\infty = 3240\ \mathrm{km\,s^{-1}}$, $\beta = 0.73$ and $\hat{r}_s = 1.011$ (or expressed equivalently to $\hat{g}_0 = 17\,392$, $\gamma = 0.46$ and $\delta = 0.68$).

The question is how these self-consistently derived wind parameters compare to earlier computations and observational constraints. First, when we employ the mass-loss recipe of Vink et al. (2000) using the stellar parameters of $T_{\mathrm{eff}} = 40\,000$ K, $M = 40.0\ M_\odot$, and $\log(L/L_\odot) = 5.5$, for an unspecified terminal wind velocity, so that the recipe uses the standard value of $v_\infty/v_{\mathrm{esc}}$ of 2.6, the recipe yields a value for the mass-loss rate of $\log \dot{M} = -5.9\ M_\odot/\mathrm{yr}$. In other words, our self-consistent computation yields a mass-loss rate in agreement with the Vink et al. recipe.

We now discuss the values that we found for the velocity field. First of all there is the shape of the velocity field, $\gamma = 0.46$ and $\delta = 0.68$, or more widely recognised as $\beta = 0.73$. This value still agrees with earlier modified CAK calculations (e.g. Pauldrach et al. 1986) as well as empirical line profile analyses (e.g. Puls et al. 1996; Mokiem et al. 2007a).

We finally turn our attention to our derived terminal wind velocity of $v_\infty = 3240\ \mathrm{km\,s^{-1}}$. This value is still in line with observations, where blue edges of P Cygni profiles do not extend beyond $\sim$3000 $\mathrm{km\,s^{-1}}$ for O star dwarfs. We assumed the same solar abundances as in Vink et al. (2000), which are based on those of Allen (1973). However, a recent 3D analysis of the solar atmosphere by Asplund (2005) suggests that the solar carbon, nitrogen, and oxygen abundances may be lower than we have assumed. As these intermediate-mass elements are important line drivers in the supersonic portion of the stellar wind (Vink et al. 1999; Puls et al. 2000), this may have implications for the outer wind acceleration, and hence might somewhat reduce the terminal wind velocity we obtain.

Our current models are non-rotating, while real O stars rotate rather rapidly. Friend & Abbott (1986) showed that the terminal wind velocity drops with equatorial rotation speed according to $v_\infty/v_{\mathrm{esc}} \propto (1-\frac{v_{\mathrm{rot}}}{v_{\mathrm{break-up}}})^{0.35}$. As O stars rotate at a significant fraction of their break-up speed, our non-rotating models provide just the upper limit to the terminal wind velocity (and the lower limit to the mass-loss rate). Further investigations, taking into account the effects of rapidly rotating O stars, predict (up to $\sim$10%) lower terminal velocities.

The above-mentioned issues will form the basis for future investigations, for which we have laid the groundwork in the present paper.

*Acknowledgements.* We thank A. de Koter for the use of his model atmospheres and R. Wehrse for helpful discussions. We acknowledge our referees, A. Feldmeier and S. Owocki, for their constructive criticism. This work was supported by PPARC/STFC.

## References

Abbott, D. C. 1980, ApJ, 242, 1183
Abbott, D. C., & Lucy, L. B. 1985, ApJ, 288, 679
Allen, C. W. 1973, Astronomical Quantities (London: The Athlone Press)
Asplund, M. 2005, ARA&A, 43, 481
Castor, J. I. 1974, MNRAS, 169, 279
Castor, J. I., & Lamers, H. J. G. L. M. 1979, ApJS, 39, 481
Castor, J. I., Abbott, D. C., & Klein, R. I. 1975, ApJ, 195, 157
Corless, R. M., Gonnet, G. H., Hare, D. E. G., & Jeffrey, D. J. 1993, Lambert's *W* Function in Maple, Maple Technical Newsletter, 9, 12
Corless, R. M., Gonnet, G. H., Hare, D. E. G., Jeffrey, D. J., & Knuth, D. E. 1996, On the Lambert *W* Function, Adv. Comput. Math., 5, 329

Cranmer, S. R. 2004, Am. J. Phys., 72, 1397
Friend, D. B., & Abbott, D. C. 1986, ApJ, 311, 701
de Koter, A., Schmutz, W., & Lamers, H. J. G. L. M. 1993, A&A, 277, 561
de Koter, A., Lamers, H. J. G. L. M., & Schmutz, W. 1996, A&A, 306, 501
de Koter, A., Heap, S. R., & Hubeny, I. 1997, ApJ, 477, 792
Gayley, K. G. 1995, ApJ, 454, 410
Gräfener, G., & Hamann, W.-R. 2005, A&A, 432, 633
Gräfener, G., Koesterke, L., & Hamann, W.-R. 2002, A&A, 387, 244
Howarth, I. D., & Prinja, R. K. 1989, ApJS, 69, 527
Kudritzki, R. P. 2002, ApJ, 577, 389
Kurucz, R. L. 1988, IAU Trans., 20b, 168
Lamers, H. J. G. L. M., & Leitherer, C. 1993, ApJ, 412, 771
Lucy, L. B. 1975, Société Royale des Sciences de Liège, Mémoires, 8, 359
Lucy, L. B. 1998, Cyclical Variability in Stellar Winds, Proceedings of the ESO Workshop, Garching, Germany, ed. L. Kaper, A. W. Fullerton, 16
Lucy, L. B. 2007a, A&A, 468, 649
Lucy, L. B. 2007b, A&A, 474, 701
Lucy, L. B., & Solomon, P. 1970, ApJ, 159, 879
Lucy, L. B., & Abbott, D. G. 1993, ApJ, 405, 738
Martins, F., Schaerer, D., & Hillier, D. J. 2005, A&A, 436, 1049
Mazzali, P. A., & Lucy, L. B. 1993, A&A, 279, 447
Mihalas, D. 1978, Stellar Atmospheres (San Francisco: Freeman)
Mihalas, D., & Weibel Mihalas, B. 1984, Foundations of Radiation Hydrodynamics (Oxford: University Press)
Mokiem, M. R., de Koter, A., Evans, C. J., et al. 2007a, A&A, 465, 1003
Mokiem, M. R., de Koter, A., Vink, J. S., et al. 2007b, A&A, 473, 603
Müller, P. E. 2001, Ph.D. Thesis, see Appendix B, Univ. of Heidelberg, Germany, www.ub.uni-heidelberg.de/archiv/1422
Parker, E. N. 1958, ApJ, 128, 664
Pauldrach, A., Puls, J., & Kudritzki, R. P. 1986, A&A, 164, 86
Puls, J. 1987, A&A, 184, 227
Puls, J., Kudritzki, R.-P., Herrero, A., et al. 1996, A&A, 305, 171
Puls, J., Springmann, U., & Lennon, M. 2000, A&A, 141, 23
Schmutz, W. 1997, A&A, 321, 268
Vink, J. S. 2000, Ph.D. Thesis, Univ. Utrecht
Vink, J. S., de Koter, A., & Lamers, H. J. G. L. M. 1999, A&A, 350, 181
Vink, J. S., de Koter, A., & Lamers, H. J. G. L. M. 2000, A&A, 362, 295
Vink, J. S., de Koter, A., & Lamers, H. J. G. L. M. 2001, A&A, 369, 574
Vink, J. S., de Koter, A., & Kotak, R. 2006, Proc. of Mass loss from stars and the evolution of stellar clusters [arXiv:astro-ph/0611749]